

# Reaction Mechanism and Surface Film Formation of Conversion Materials for Lithium- and Sodium-Ion Batteries: An XPS Case Study on Sputtered Copper Oxide (CuO) Thin Film Model Electrodes

Franziska Klein,<sup>†</sup> Ricardo Pinedo,<sup>†</sup> Philipp Hering,<sup>‡</sup> Angelika Polity,<sup>‡</sup> Jürgen Janek,<sup>†</sup> and Philipp Adelhelm<sup>\*,§</sup>

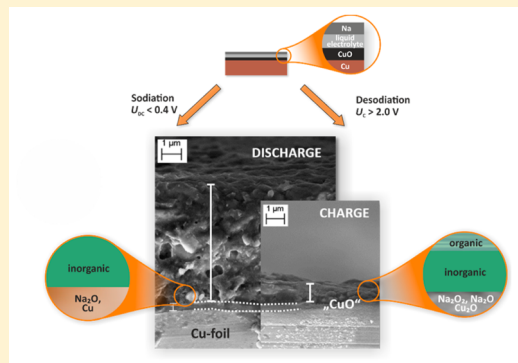
<sup>†</sup>Justus-Liebig-University Giessen, Institute of Physical Chemistry, Heinrich-Buff-Ring 17, 35392 Giessen, Germany

<sup>‡</sup>Justus-Liebig-University Giessen, 1st Physics Institute, Heinrich-Buff-Ring 16, 35392 Giessen, Germany

<sup>§</sup>Friedrich-Schiller-University Jena, Institute for Technical Chemistry and Environmental Chemistry, Center for Energy and Environmental Chemistry (CEEC), Philosophenweg 7a, 07743 Jena, Germany

## Supporting Information

**ABSTRACT:** Charge storage based on conversion reactions is a promising concept to store electrical energy. Many studies have been devoted to conversion reactions with lithium; however, still many scientific questions remain due to the complexity of the reaction mechanism combined with surface film formation. Replacing lithium by sodium is an attractive approach to widen the scope of conversion reactions and to study whether the increase in ion size changes the reaction mechanisms and whether the cell performance benefits or worsens. In this study, we use thin film electrodes as a additive-free model system to study the conversion reaction of CuO with sodium (CuO/Na) by means of electrochemical methods, microscopy, and X-ray photoelectron spectroscopy. The reaction mechanism and film formation are being discussed. Some important differences to the analogue lithium-based system (CuO/Li) are found. Whereas CuO has been reported as charge product in CuO/Li cells, charging is incomplete in the case of CuO/Na and only Cu<sub>2</sub>O is formed. As an important finding, oxygen appears to be redox active and Na<sub>2</sub>O<sub>2</sub> forms during charging from Na<sub>2</sub>O. Moreover, surface film formation due to electrolyte decomposition is much more severe as compared to CuO/Li. Depth profiling is used to probe the inner composition of the surface film, revealing a much thicker surface film with more inorganic components as compared to the lithium system. It is also found that the surface film disappears to a large extent during charging.



## 1. INTRODUCTION

Electrochemical energy stores play a vital role in our present society, and their relevance will further grow as numerous technologies require solutions for the safe, compact, and affordable storage of electrical energy on a local scale. Successive improvement of lithium-ion batteries (LIBs) is an important route to fulfill the forthcoming needs; however, also a range of alternative cell systems are currently being studied that aim at overcoming some intrinsic limitations related to conventional lithium-ion intercalation chemistry.

Well-known examples are the so-called “next-generation” systems lithium–sulfur (Li/S) and lithium–oxygen (Li/O<sub>2</sub>). Their theoretical energy densities are several times higher than state-of-the-art Li-ion technologies.<sup>1</sup> However, sufficient reversibility under practical conditions has not been achieved to date yet. This is mainly due to the complex chemistry at the positive (sulfur or oxygen) electrode, issues related to lithium metal as negative electrode, and the instability of the available organic electrolytes. Conversion reactions based on the full reduction/oxidation of mostly transition metals—leading to the

transfer of several electrons—are another candidate for “next-generation” systems.<sup>2</sup> A wide range of compounds such as transition metal oxides, sulfides, fluorides, nitrides, and phosphides are being tested for application for anodes as well as cathodes. If commercialized, high capacities and hence high energy density cells could be realized. Nevertheless, also here, the cell chemistry is complex and a number of unsolved challenges such as insufficient cycle life and large overpotentials hinder the practical application of these materials for rechargeable room-temperature battery systems.<sup>3</sup>

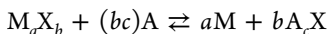
Despite the progress of lithium battery technology, lithium is merely in the 27th place in the table of abundance of chemical elements and, therefore, in principle, exhaustible.<sup>4,5</sup> Whether this will become a limiting factor for LIB technology in the future is, however, a more political question as the resources are unequally distributed around the world. But, as the develop-

Received: October 30, 2015

Revised: December 14, 2015

ment time of batteries is very long, it is necessary to study potential alternatives as early as possible. Sodium is a conceivable option because of its comparable physical and chemical properties. Additionally, sodium is abundant and, therefore, an ideal candidate when aiming at low-cost battery cell concepts.<sup>1,4,6–14</sup> From a practical perspective, one might speculate, whether replacing lithium by sodium in “next-generation” systems might help to overcome some of the current challenges. Comparing Li/O<sub>2</sub> and Na/O<sub>2</sub> cells, for example, the sodium cell shows significant advantages, though at the expense of energy density. On the other hand, for low temperature Na/S cells, the performance so far seems much poorer as compared to Li/S cells.<sup>1</sup> Scientifically, the question of how the replacement of lithium by sodium influences the cell chemistry is quite intriguing, and indeed substantial differences should occur also for conversion reactions with transition metals.<sup>15</sup>

With lithium or sodium as counter electrode the idealized conversion reaction of a compound M<sub>a</sub>X<sub>b</sub> can be written as



with M being a transition metal (or Mg), X a nonmetal (i.e., O, S, F, P, N, ...), and A the alkali metal (Li or Na), respectively.

Commonly, conversion electrodes are prepared in the delithiated (desodiated) state, so the first reaction proceeds from left to right. During discharge, a network of transition metal nanoparticles (M) embedded in a matrix of the alkali compound (A<sub>c</sub>X) forms. The process is reversed during charging.<sup>3,16</sup>

A broad range of conversion reactions based on sodium has been studied so far: oxides (CuO,<sup>17–23</sup> Co<sub>3</sub>O<sub>4</sub>,<sup>24–27</sup> NiO,<sup>28</sup> Fe<sub>3</sub>O<sub>4</sub>,<sup>29–32</sup> Fe<sub>2</sub>O<sub>3</sub>,<sup>33–41</sup> MoO<sub>3</sub>,<sup>42</sup> WO<sub>3</sub>,<sup>43</sup>) sulfides (CoS<sub>2</sub>,<sup>44</sup> Co<sub>3</sub>S<sub>4</sub>,<sup>45</sup> FeS<sub>2</sub>,<sup>46–48</sup> WS<sub>2</sub>,<sup>43,49</sup> MoS<sub>2</sub>,<sup>50–60</sup> Ni<sub>3</sub>S<sub>2</sub>,<sup>61–64</sup> Cu<sub>2</sub>S<sup>65</sup>), fluorides (CoF<sub>2</sub>,<sup>66</sup> phosphides (NiP<sub>3</sub>,<sup>67</sup>), nitrides (VN,<sup>68</sup> Ni<sub>3</sub>N<sup>69</sup>), selenides (FeSe,<sup>70</sup> MoSe,<sup>71</sup> Cu<sub>2</sub>Se<sup>72</sup>), and ternary systems (FeV<sub>2</sub>S<sub>4</sub>,<sup>73</sup> Mo<sub>3</sub>Co<sub>6</sub>S<sub>8</sub>,<sup>74</sup> titanates,<sup>75</sup> NiCo<sub>2</sub>O<sub>4</sub>,<sup>76</sup>). Their cell chemistry has been found to be complex in all cases. Compared to the lithium counterparts, the cell voltage is mostly (but not always)<sup>15</sup> lower for the sodium system, the experimentally determined capacities are lower (poor utilization of active material), and the volume expansion is naturally larger due to the larger ion radius of Na<sup>+</sup>. Differences in the reaction mechanism, however, are much more difficult to unravel, which mostly relates to the nanostructured nature of the electrode after intercalation. Different reaction mechanisms for the conversion reactions of NiO with Li and Na have been recently observed by He et al.<sup>77</sup> Another yet (for lithium- and sodium-based conversion reactions) poorly understood phenomenon is the surface film formation that appears during the first intercalation. We will use the term solid electrolyte interphase (SEI) for this surface film; although, also different names such as “gel-like polymeric” film have been used.<sup>3</sup> Interestingly, it has been found that the SEI on conversion materials partly disappears during delithiation, the reason though remains speculative.<sup>78</sup> Several analytical methods might be applied to study the structural evolution of conversion reactions, but a practical hurdle is that the electrodes usually contain larger amounts of carbon conductive additives (typically 15–25 wt %) and binder that are necessary to achieve a reasonable electrode activity. Combined with the rough surface of particle based electrodes, many surface sensitive methods are, therefore, difficult to apply. Much better

suit for analysis are thin film electrodes, as no additives are necessary and their surface is usually reasonably well-defined.

In this study, we focus on the surface film formation and cell reaction of the conversion reaction between CuO thin films with lithium and sodium, respectively. CuO has been chosen, as it has been already applied in primary cells<sup>79–85</sup> and is currently also studied as thin film material for solar cells. Some of the authors have extended experience in preparing such films by sputtering methods.<sup>86,87</sup>

Different forms of CuO electrodes such as films, nanowires, nanorod arrays, and micro-nanostructured CuO/C spheres have been electrochemically characterized.<sup>17–23</sup> It was confirmed by *ex situ* XRD, Raman, and TEM measurements that, during the first sodiation, the conversion reaction of CuO involves the formation of elemental Cu and Na<sub>2</sub>O. Cu<sub>2</sub>O forms as intermediate phase. Lui et al. proposed NaCuO and Na<sub>6</sub>Cu<sub>2</sub>O<sub>6</sub> as additional discharge products by *in situ* TEM experiments.<sup>18</sup> During charging, some authors confirmed the reappearance of CuO,<sup>17,22,23</sup> whereas others exclusively found Cu<sub>2</sub>O<sup>21</sup> or “6CuO·Cu<sub>2</sub>O”.<sup>20</sup> Thus, owing to these partly controversial results, the cell reaction between CuO and sodium needs thorough enlightenment. It is also important to note that the first cycle in an electrochemical experiment is not representative for the subsequent ones as conversion electrodes always undergo an initial activation (see Figure 1). The

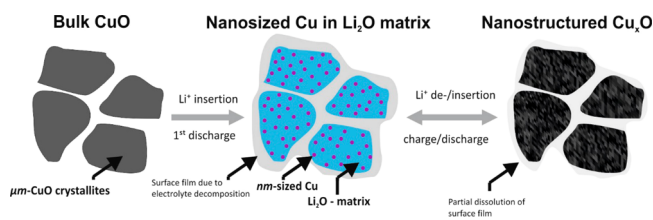


**Figure 1.** Sketch of the generally accepted reaction mechanism of conversion reactions using the example CuO/Li. During the first lithiation, a complex nanostructure develops with copper nanoparticles dispersed in an amorphous matrix of Li<sub>2</sub>O. This nanocomposite shows partial reversibility in the subsequent cycles. The reaction is accompanied by side reactions with the electrolyte leading to surface film formation.

reversibility of the electrode reaction is, therefore, better studied after the electrode has been cycled for a few times. In this paper, we focus on the 10th rather than the 1st cycle and use XPS to study the electrode reaction.

So far, XPS has been applied to study the conversion reaction of CuO with lithium only.<sup>88,89</sup> Martin et al. showed for CuO thin film electrodes that Cu<sub>2</sub>O and Li<sub>2</sub>O<sub>2</sub> form as intermediates and Cu and Li<sub>2</sub>O as end products during lithiation in the first cycle. Along with this process, electrolyte decomposition led to an organic/inorganic surface film. The inorganic layer consisted of LiF and resulted from decomposition of the electrolyte conducting salt LiPF<sub>6</sub>, while the organic, polymeric outer surface resulted from the decomposition of the carbonate solvent. During charging, Cu was only oxidized to Cu<sub>2</sub>O and so Li<sub>2</sub>O to Li<sub>2</sub>O<sub>2</sub>. The organic part of the surface film disappeared and only LiF remained. Upon subsequent cycling, however, a continuous growth of the polymeric film was observed.

Although most studies on conversion have focused on characterizing the reaction mechanism, it is clear that understanding the formation of the surface films (SEI) is just as important. Only a stable surface film will enable long cycle life without the need for excess electrolyte. Only little attention

has been paid on this aspect, especially for conversion reactions with sodium. Only a few studies have been published so far. A study of Komaba et al. on carbon electrodes showed that the SEI in the case of sodium contains more inorganic components and is more homogeneously structured than in the case of lithium, with inorganic carbonates as the main component.<sup>90,91</sup> Depending on the system employed, the thickness varies from 5 to 10 nm (e.g., for hard carbons and  $\text{Na}_2\text{Ti}_3\text{O}_7$ ) and is, therefore, thinner than in the lithium counterpart.<sup>91,92</sup> For sodium, Edström et al. found a remarkably thick SEI for the conversion system  $\text{Fe}_2\text{O}_3/\text{Na}$  by means of soft X-ray photoelectron spectroscopy (PES).<sup>93</sup> Depth profiling is, therefore, necessary to study the SEI composition and the buried electrode.

This study aims at characterizing the conversion reaction of CuO thin film electrodes with sodium as well as the accompanying surface film formation. Cycling voltammetry and galvanostatic cycling are used as electrochemical methods; SEM is used to study morphological changes. XPS combined with depth profiling is used to study the spatial composition and formation of the SEI layer. The results are compared with the analogous Li-based conversion reaction.

## 2. EXPERIMENTAL SECTION

### 2.1. Preparation of Free-Standing CuO Thin Film Electrodes.

Cupric oxide (CuO) thin films were prepared by reactive radio frequency sputtering in a mixed ( $\text{Ar} + \text{O}_2$ ) atmosphere, utilizing a 3" metallic copper target. The RF power applied to the target was set to 50 W, resulting in a density of  $1.1 \text{ W cm}^{-2}$ . The working argon and reactive oxygen gas flow rates were kept at 55 and 5 sccm, respectively, adding up to a working pressure of  $10^{-2}$  mbar. With those parameters, the sputtering process yields spatially homogeneous cupric oxide thin films at a deposition rate of  $6 \text{ nm min}^{-1}$ , where the deposition time was chosen to result in film thicknesses of  $\sim 200 \text{ nm}$ .

### 2.2. Structural and Morphological Characterization of CuO Thin Films.

The structural properties of the CuO thin films were studied by means of X-ray diffraction (XRD) using an X'Pert Pro (PANalytical) powder X-ray diffractometer (Cu-K source, 40 kV, 40 mA), while their cross-sectional and surface morphologies were investigated by scanning electron microscopy (SEM) using a Merlin high-resolution Schottky field-emission electron microscope (Zeiss SMT).

### 2.3. Cell Assembly and Electrochemical Measurements.

The prepared CuO thin film electrodes were assembled in Swagelok-type T-cells (3-electrode configuration) in an Ar-filled glovebox keeping the oxygen and water levels below 1 ppm. CuO thin film electrodes were used as working electrodes with metallic lithium or sodium acting as counter and reference electrodes. Both, Whatman and Celgard separators were placed between counter and working electrodes and were soaked with 80  $\mu\text{L}$  of electrolyte, meaning 0.5 M NaFSI (sodium-bis(fluorosulfonyl)imide) in EC/DMC (3:7, v/v) (ethylene carbonate, dimethylcarbonate) as sodium-based electrolyte and LiPF<sub>6</sub> in EC/DMC (LP30, battery grade, Merck, <10 ppm of H<sub>2</sub>O) in the case of Li half-cells. The sodium conducting salt was dried at 120 °C under vacuum for 24 h while the solvents were dried over molecular sieves for at least 72 h. NaFSI was chosen as conductive salt because we found the overall stability and reproducibility to be better for the sodium cell as compared to when other salts such as NaPF<sub>6</sub> were used (see Figure S.I.1).

Bulk-electrodes were prepared as follows: 65 wt % active material (CuO, Sigma-Aldrich), 25 wt % conducting additive (Super PLi, Timcal), and 10 wt % binder (NaCMC, Sigma-Aldrich) were mixed to a slurry, stirred for 24 h, and casted onto a copper foil (Schlenk) by doctor blading. The prepared electrodes were then dried under vacuum and pressed.

Cyclic voltammetry (CV) was performed via a VMP3 equipment (Bio-Logic) by applying a scan rate of  $0.05 \text{ mV s}^{-1}$  in the voltage range of 0.01–3.0 V vs Na/Na<sup>+</sup> or vs Li/Li<sup>+</sup> for both types of half-cells. Galvanostatic measurements were conducted in a MacCor battery cycler (Series 4000) employing a constant current of  $10 \mu\text{A}$ . Several cutoff voltages were selected in order to investigate the evolution of the surface layer at different states of discharge/charge and cycles. Thus, the defined cutoff potentials during the 1st and 10th cycles were 0.01 V ("full discharge") and 3.0 V ("full charge"). Moreover, 0.4 V vs Na/Na<sup>+</sup> and 0.84 V vs Li/Li<sup>+</sup> cutoff voltages were specifically chosen as a partially first discharged state and 2.2 V vs Na/Na<sup>+</sup> and Li/Li<sup>+</sup> as the comparative charged state. It is worth noting that, at the partially dis/charged states, only Cu<sub>2</sub>O is expected.<sup>94</sup> All electrochemical experiments were carried out at a constant and controlled temperature of 25 °C.

**2.4. Morphological Characterization.** Cells were disassembled under Ar atmosphere, and electrodes were rinsed with dried EC/DMC (3:7, v/v) solvent to remove the remaining conducting salt from the surface. Subsequently, samples were dried in vacuum for 3 h under mild conditions (i.e., 65 °C) in order to preserve the morphology. The electrodes were then transferred from the glovebox to the spectrometer and/or SEM by transfer systems under an inert argon atmosphere, avoiding air exposure.

**2.5. X-ray Photoelectron Spectroscopy (XPS) Analysis.** X-ray photoelectron spectroscopy (XPS) measurements were carried out with a PHIS000 Versa Probe spectrometer using a monochromatic Al K $\alpha$  radiation ( $h\nu = 1486.6 \text{ eV}$ ). The peaks were recorded with a constant pass energy of 23.5 eV. The diameter of the irradiated area was  $\sim 200 \mu\text{m}$ . To minimize charging effects, a dual beam charge neutralization system was used. For sputtering and depth profiling, an Ar beam with an applied voltage of 1 kV was employed.

Photoelectron spectra were fitted with a Casa XPS software with Shirley backgrounds and 100% Gaussian curves. All spectra were charge corrected to a binding energy from hydrocarbons contamination on top of the surface using the C 1s peak at 284.6 eV. During etching, the F 1s line at 683.5 eV corresponding to NaF was used for further corrections since the hydrocarbons do not provide a reliable reference line. Quantification was performed on the basis of Scofield's relative sensitivity factors (R.S.F. values).

## 3. RESULTS AND DISCUSSION

### 3.1. General Aspects of the Electrode Reaction.

Conversion reactions proceed in a very particular way which is mainly related to the fact that a complex nanostructure develops during the first lithiation (or sodiation) process. The generally accepted mechanism is sketched in Figure 1 for the lithiation of CuO. The nanocomposite provides intimate contact between the active phases and is an important reason for the electrode remaining electrochemically active during cycling despite the poor conductivity of most phases involved.

Although conversion reactions show relatively large overpotentials leading to hysteresis during cycling, it is important to recall the theoretical redox potentials at which the reaction

**Table 1.** Thermodynamic Values Derived from HSC Chemistry 8.0 ( $p = 10^5$  Pa,  $T = 25$  °C, Bulk Thermodynamics, Pure Phases)<sup>a</sup>

|   | lithium   | $\Delta_f G^\circ$ (25 °C)/kJ mol <sup>-1</sup> | $E^\circ$ vs Li/Li <sup>+</sup> | $w_{th}/\text{Wh kg}^{-1}$ | volume change/% | $q_{th}/\text{mAh g}^{-1}$ |
|---|---|---|---------------------------------|----------------------------|-----------------|----------------------------|
| A | $2\text{Li} + \text{CuO} \rightarrow \text{Li}_2\text{O} + \text{Cu}$               | -431.551  | 2.24                            | 1285                       | +74             | 674                        |
| B | $2\text{Li} + \text{Cu}_2\text{O} \rightarrow \text{Li}_2\text{O} + 2\text{Cu}$     | -413.302  | 2.14                            | 731                        | +22             | 375                        |
| C | $2\text{Li} + 2\text{CuO} \rightarrow \text{Li}_2\text{O}_2 + 2\text{Cu}$           | -311.625  | 0.81                            | 500                        | +35             | 674                        |
| D | $2\text{Li} + 2\text{Cu}_2\text{O} \rightarrow \text{Li}_2\text{O}_2 + 4\text{Cu}$  | -275.128  | 0.71                            | 255                        | +1              | 375                        |
| E | $2\text{Li} + 4\text{CuO} \rightarrow \text{Li}_2\text{O}_2 + 2\text{Cu}_2\text{O}$ | -348.123  | 0.90                            | 291                        | +34             | 337                        |
| F | $2\text{Li} + 2\text{CuO} \rightarrow \text{Li}_2\text{O} + \text{Cu}_2\text{O}$    | -449.800  | 2.33                            | 722                        | +54             | 337                        |
|   | sodium  | $\Delta_f G^\circ$ (25 °C)/kJ mol <sup>-1</sup> | $E^\circ$ vs Na/Na <sup>+</sup> | $w_{th}/\text{Wh kg}^{-1}$ | volume change/% | $q_{th}/\text{mAh g}^{-1}$ |
| G | $2\text{Na} + \text{CuO} \rightarrow \text{Na}_2\text{O} + \text{Cu}$               | -246.705  | 1.28                            | 546                        | +173            | 674                        |
| H | $2\text{Na} + \text{Cu}_2\text{O} \rightarrow \text{Na}_2\text{O} + 2\text{Cu}$     | -228.456  | 1.18                            | 336                        | +74             | 375                        |
| I | $2\text{Na} + 2\text{CuO} \rightarrow \text{Na}_2\text{O}_2 + 2\text{Cu}$           | -190.531  | 0.49                            | 258                        | +67             | 674                        |
| J | $2\text{Na} + 2\text{Cu}_2\text{O} \rightarrow \text{Na}_2\text{O}_2 + 4\text{Cu}$  | -154.034  | 0.40                            | 129                        | +18             | 375                        |
| K | $2\text{Na} + 4\text{CuO} \rightarrow \text{Na}_2\text{O}_2 + 2\text{Cu}_2\text{O}$ | -227.029  | 0.59                            | 173                        | +49             | 337                        |
| L | $2\text{Na} + 2\text{CuO} \rightarrow \text{Na}_2\text{O} + \text{Cu}_2\text{O}$    | -264.954  | 1.37                            | 359                        | +103            | 337                        |
| M | $\text{Na} + 2\text{CuO} \rightarrow \text{Na}_2\text{O}_2 + 2\text{Cu}$            | +40.433   | -0.10                           | -62                        | +55             | 337                        |
| N | $\text{Na} + 2\text{Cu}_2\text{O} \rightarrow \text{Na}_2\text{O}_2 + 4\text{Cu}$   | +76.930   | -0.20                           | -69                        | +12             | 187                        |
| O | $\text{Na} + 4\text{CuO} \rightarrow \text{Na}_2\text{O}_2 + 2\text{Cu}_2\text{O}$  | +3.935  | -0.01                           | -3                         | +44             | 168                        |

<sup>a</sup>Values for theoretical energy densities ( $w_{th}$ ) are calculated with respect to the total mass of all elements included, i.e., Li, Na, Cu, O. Theoretical capacities ( $q_{th}$ ) relate to the active electrode mass that is the copper compounds only. Note that, due to the low redox potentials (C–L), CuO is a negative electrode material considering application.

should occur as well as the emerging volume changes. From the different thermodynamically stable phases,<sup>95</sup> a range of possible reactions can be considered as shown in Table 1. Starting from CuO, reactions A and G represent the ideal case, i.e., full reduction of Cu(II) and formation of the oxide. Several more reactions (B–F and H–L) might take place when only partial conversion (especially during cycling) takes place.

The theoretical redox potentials vs the corresponding alkali metal electrode can be readily derived from the reaction equations. With the exception of reactions A, B, and F, reactions C–L can clearly only serve as negative electrodes in practical cells. Voltages are systematically lower in the case of sodium, as has been discussed earlier.<sup>15</sup> In the case of sodium, the superoxide NaO<sub>2</sub> is stable as well next to the oxide and peroxide. However, reactions including NaO<sub>2</sub> as discharge product have a positive Gibbs energy and are, therefore, not expected to occur. Note that the tabulated thermodynamic data for NaO<sub>2</sub> might not be completely accurate as the phase is chemically difficult to synthesize. Therefore, a slight driving force might not be impossible. Moreover, also nanoscale effects (influence of surface energy, nucleation barriers, etc.) and solid solution behavior might lead to deviations from bulk thermodynamics.

Besides, a range of other kinetic and/or thermodynamic factors related to the ion size can influence the reversibility of the conversion reaction. A common issue for conversion reactions, which strongly affects the degree of reversibility, is the volume expansion as stress and strain can lead to mechanical instabilities of the electrode. Volume expansion is more severe in the case of sodium due to the larger ionic radius compared to lithium.<sup>15</sup> The smallest volume changes are found for reaction D (+1%) and J (+18%), which might favor reversibility of the electrode reaction as long as other reactions do not take place. The reversibility of the individual reactions between CuO ↔ Cu<sub>2</sub>O ↔ Cu are still under debate in the case of lithium and are even more unclear in the case of sodium. Usually, the sodium cells show lower practical capacities and a shorter cycle life as the analogue lithium systems. The argument put forward is in most cases the huge volume

change during these reactions which, as previously commented, is significantly larger for Na-based reactions, and the result is a decay in the specific capacity. Thus, if conversion reactions seem to be not fully reversible in Li-systems, the possibility that they are not reversible in Na-systems appears more than reasonable at first glance. Nevertheless, considering the complexity of the nanostructure (Figure 1), reversibility of the electrode will depend on many factors and on each individual system. A too high diffusion coefficient of one of the reaction partners can also counteract the reversibility, for example.<sup>96</sup> Some more direct advantages for the sodium systems are related to the solvation properties. This argument has been reported as a reason to explain the lower viscosity and higher conductivity of Na solutions with aprotic solvents, for example.<sup>4</sup> Moreover, theoretical studies pointed out that the desolvation energy of a sodium ion is commonly smaller by ca. 40–70 kJ mol<sup>-1</sup>.<sup>97</sup> This suggests much lower activation barriers of Na-ion insertion into solid electrodes, as also shown experimentally by Sagane et al.,<sup>98</sup> and could enable faster charge–discharge kinetics of SIBs compared to LIBs. Another important factor that influences the redox activity of conversion reactions is the conductivity (ionic and electronic) of the materials. Oxides are mainly insulators (Li<sub>2</sub>O, Na<sub>2</sub>O, Li<sub>2</sub>O<sub>2</sub>, Na<sub>2</sub>O<sub>2</sub>), and NaO<sub>2</sub> is likely a poor semiconductor.<sup>99–101</sup> CuO and Cu<sub>2</sub>O are semiconductors with band gaps of  $E_g(\text{Cu}_2\text{O}) = 2.1$  eV,  $E_g(\text{CuO}) = 1.4$  eV at room temperature. Nevertheless it is worth noting that conductivity can increase due to nonstoichiometry. The conductivity in CuO thin films can vary several orders of magnitude, for example.<sup>86</sup> Also, the formation of other defects that might enable ionic conduction will differ between lithium and sodium systems.

Overall, the range of possible reactions clearly shows how challenging the correct determination of the electrode reaction becomes. Additionally significant overpotentials and hence a shift of the redox potentials are expected due to the often poor kinetics of solid state phase transitions and the poor conductivity of the materials involved. Redox processes due to electrolyte decomposition further complicate the situation. As a result, the use of cyclic voltammetry to determine the cell

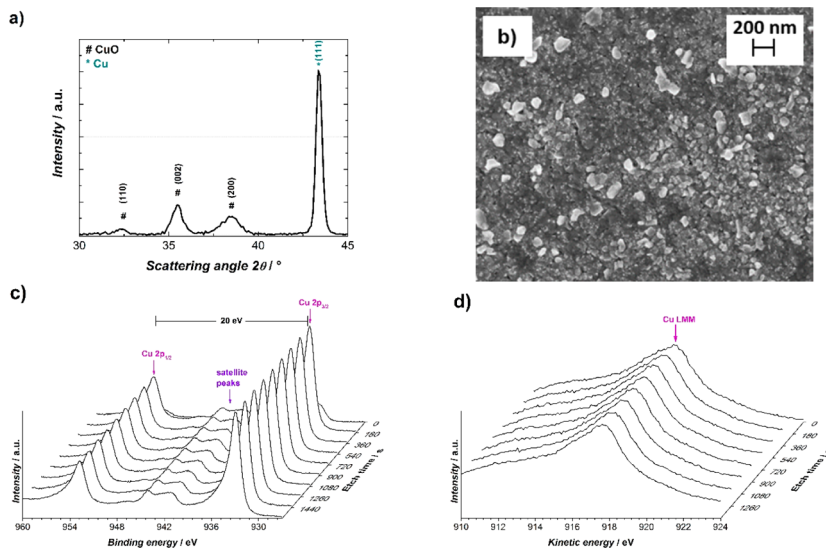


**Figure 2.** (a) XRD patterns, (b) surface morphology, and (c, d) XPS depth profile analyses of the as-deposited CuO thin films.

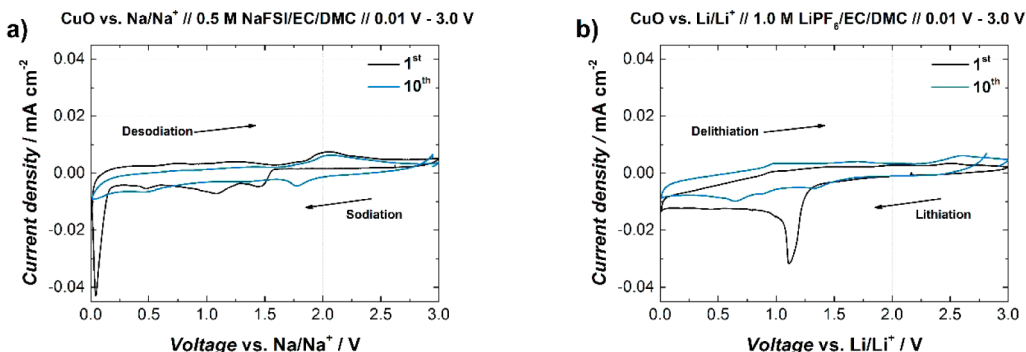


**Figure 3.** Cyclic voltammograms of CuO thin film electrodes for (a) Na and (b) Li half-cells in the potential range of 0.01–3.0 V vs A/A<sup>+</sup> (A = Na, Li) obtained during the 1st and 10th cycles.

reaction is limited as only very broad and ill-defined voltammograms are found (see section 3.3).

**3.2. Characterization of CuO Thin Film Electrodes.** CuO thin film electrodes were first characterized by means of X-ray diffraction (see Figure 2a). Both, CuO and Cu were identified, the latter being due to the employed Cu substrate. CuO reflections can be indexed on the basis of a monoclinic phase (ICSD No. 800076), and no impurities were detected. The broad signals indicate nanocrystallinity. The average crystallite size of the copper oxide is around 13 nm, as estimated using the Scherrer equation. Morphological characterization of the surface and cross section of the CuO thin films was conducted by SEM (Figure 2b and Figure S.I.2, SI).

Homogeneously distributed CuO particles with sizes in the range of 10–80 nm were observed, and the layer thickness reaches approximately 200 nm. XPS analyses (Figure 2c,d) of the Cu 2p core level reveal the presence of several peaks at about 933.6, 940–944, and 953 eV. The main Cu 2p<sub>3/2</sub> peak at 932.6 eV and the corresponding Cu 2p<sub>1/2</sub> peak shifted to 20 eV higher binding energies are due to CuO.<sup>102</sup> Satellite peaks in the region of 940–944 eV are clearly visible, providing further evidence of the presence of CuO, as this satellite feature is an indication of materials having a partially filled d<sup>9</sup> shell configuration in the ground state, such as CuO.<sup>103,104</sup> For Cu<sub>2</sub>O with a completely filled shell (d<sup>10</sup>), these satellite peaks are absent because screening via a charge transfer into the d

states is not allowed.<sup>105</sup> It is worth noting that no significant shifts are observed for the Cu 2p spectra and the Cu LMM Auger peak, located at 917.9 eV, during the depth profile analysis, confirming that the oxidation state of CuO is kept even after the etching process.

**3.3. Cyclic Voltammetry.** Cyclic voltammetry analyses were conducted in order to shed some light on the electrochemical processes of CuO thin film electrodes in both sodium- and lithium-based half-cells (see Figure 3). A slow scan rate of 0.05 mV s<sup>-1</sup> was selected to separate all electrochemical processes.

For the CuO/Na-system, three weak reduction peaks at 1.45, 1.08, and 0.48 V vs Na/Na<sup>+</sup> can be noticed during the 1st cycle. The reduction peak at 1.45 V can be related to the formation of a solid solution, while those at 1.08 and 0.48 V are ascribed to the Cu(II) to Cu(I) and Cu(I) to metallic Cu reduction processes, respectively.<sup>20,23</sup> The intense current close to 0 V is due to electrolyte decomposition.<sup>91,92,106</sup> Extending the analysis to further cycles reveals that the main differences are found during reduction where the peak at 1.45 V is shifted to higher potentials (1.78 V) and the peak at 1.08 and 0.04 V largely disappear. During oxidation (charging), the differences between the 1st and 10th cycles are less obvious. The most well-defined peak around 2.0 V remains largely unchanged. Overall, it can be seen that the 1st cycle and 10th cycle (stabilized state) deviate

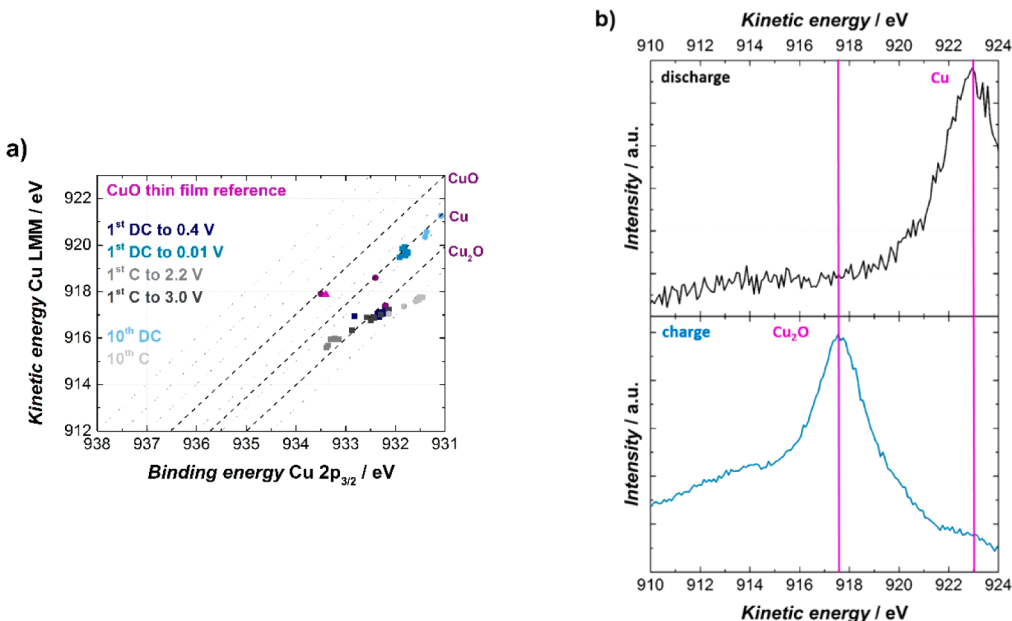


**Figure 4.** (a) Wagner plot from data of the CuO/Na-system at different states of discharge and charge and cycles. (b) Cu LMM Auger peak after the 10th dis/charge and 720 s sputter time.

especially with respect to the reduction sweep. This is well in line with the activation of the electrode according to Figure 1.

For the CuO/Li-system, the most significant feature during the first cycle is the reduction peak located at 1.2 V, usually associated with the reduction of CuO to Cu<sub>2</sub>O but also to the decomposition of the electrolyte. This peak is clearly irreversible. No further defined peaks appear during reduction in the first cycle. However, a constant negative current of around  $-15 \mu\text{A cm}^{-2}$  flows when approaching 0 V vs Li/Li<sup>+</sup>. The current remains negative even when starting the anodic sweep, indicating that a slow and continuous degradation mechanism takes place at low potentials. Upon subsequent cycling, the reduction peaks due to CuO  $\rightarrow$  Cu<sub>2</sub>O and Cu<sub>2</sub>O  $\rightarrow$  Cu transitions (1.4 and 0.85 V, respectively) and the electrolyte decomposition (0.5 V) become also evident, in good agreement with previous reports.<sup>107</sup>

Because of the complexity of the electrode reaction, only a few qualitative statements can be concluded from CV experiments: (1) The activation of the electrode during the first lithiation/sodiation can be clearly seen in the voltammogram. (2) In the case of sodium, rapid electrolyte decomposition appears close to 0 V. (3) In the case of lithium, the electrolyte decomposition might be a slower and more continuous process. (4) Peaks associated with electrolyte decomposition decrease upon cycling (although this does not mean that continuous decomposition takes place).

**3.4. Reaction Mechanism and Film Formation.** Because of its high chemical sensitivity, XPS measurements combined with depth profiling provide important information for understanding not only the reaction mechanism but also the SEI formation/dissolution process. Both processes will be examined in the following sections. Results from XPS are further correlated with galvanostatic cycling data.

**3.4.1. Reaction Mechanism and Cycle Life.** The so-called Wagner plot depicts the kinetic energy of the Cu Auger peak against the binding energy of the Cu 2p peak (see Figure 4a). Thus, the chemical state of copper corresponds to a specific linear relationship between the Auger energy and the

photoemission energy.<sup>108</sup> In consequence, copper reaction products have been identified by Wagner plots at different states of discharge (0.4 and 0.01 V vs Na/Na<sup>+</sup>) and charge (2.2 and 3.0 V vs Na/Na<sup>+</sup>) during the 1st and 10th cycles. The chemical oxidation state of Cu was evaluated after each sputter process in order to examine the reaction products along the depth profile (Figure 4b and Figure S.I.3, SI). Note that the sputter depth cannot be simply calculated from the sputter time. This is because the sputter yield is not known due to the complex microstructure of the electrode. However, from the results discussed below, it is clear that the sputter time was long enough to penetrate any surface film. The copper current collector was not reached during sputtering.

Attending to the Wagner plot shown in Figure 4a, the following copper reaction products during the 1st and 10th cycles have been determined (Table 2).

**Table 2. Copper Reaction Products in CuO/Na Conversion Electrodes Deduced from the Wagner Plot during the 1st and 10th Cycles**

| cycle | discharge/charge | depth of discharge/charge (V) | copper reaction product |
|-------|------------------|-------------------------------|-------------------------|
| 1st   | discharge        | 0.40                          | Cu <sub>2</sub> O       |
| 1st   | discharge        | 0.01                          | Cu                      |
| 1st   | charge           | 2.20                          | Cu <sub>2</sub> O       |
| 1st   | charge           | 3.00                          | Cu <sub>2</sub> O       |
| 10th  | discharge        | 0.01                          | Cu                      |
| 10th  | charge           | 3.00                          | Cu <sub>2</sub> O       |

During the first cycle, CuO is initially reduced to Cu<sub>2</sub>O (0.4 V vs Na/Na<sup>+</sup>) and subsequently to Cu (0.01 V vs Na/Na<sup>+</sup>). However, Cu is only reoxidized to Cu<sub>2</sub>O during the following charge. The Wagner plot does not show mixed chemical states such as Cu<sub>3</sub>O<sub>4</sub> and CuO seems not to be formed during charge. This phase sequence is maintained during further cycles in good agreement with the doublet (1.78–2.06 V) observed in the CV analysis. Overall, the results clearly evidence reversible

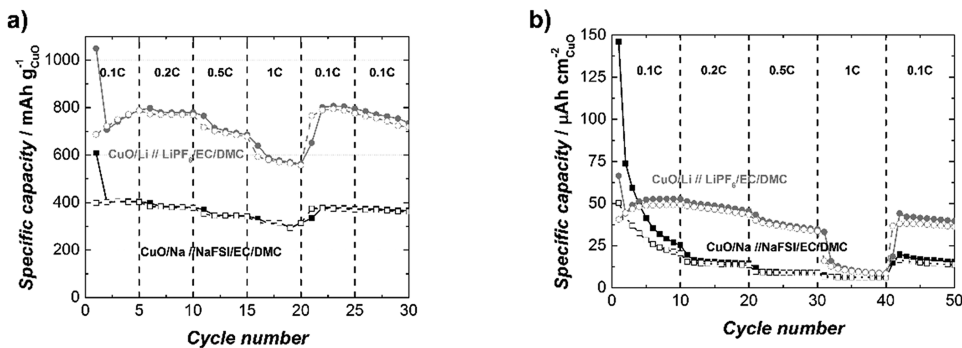


**Figure 5.** Rate performance of CuO electrodes in lithium and sodium cells with (a) bulk electrodes and (b) thin films. The C-rate is calculated for the ideal case of full conversion of CuO; i.e., 1C corresponds to 674 mA g<sup>-1</sup>.

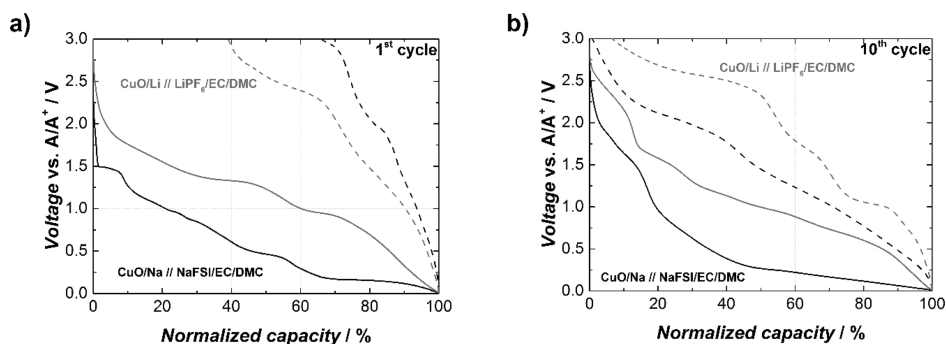


**Figure 6.** Normalized voltage profiles of the CuO thin film electrodes for the 1st and 10th cycles.

conversion between Cu<sub>2</sub>O and Cu only (reaction H, Table 1) and not between CuO and Cu (reaction G, Table 1). This is in contrast to some earlier studies on CuO/Na cells where full reversibility was proposed based on CV, *ex situ* XRD, and Raman measurements.<sup>19,22,23</sup> Considering the limitation of reaching only Cu<sub>2</sub>O during charging, the theoretical reversible capacity of the CuO electrode, therefore, decreases from 674 to 337 mAh g<sup>-1</sup> (a Cu<sub>2</sub>O electrode has a theoretical capacity of 375 mAh g<sup>-1</sup>). It is worth noting that the behavior of the present CuO/Na cells seems different from CuO/Li. Several groups have reported at least partial reoxidation from Cu<sub>2</sub>O to CuO in the case of lithium; i.e., reaction A occurs at least to some extent.<sup>3,78,88,109</sup> Moreover, different types of microstructures are commonly reported in the literature<sup>94,110</sup> and could complicate the comparisons as this fact seems to play also an important role due to the favorable accommodation of volume changes in porous spaces during lithium insertion reaction.<sup>111</sup>

We, therefore, performed the same XPS depth profiling experiments for the CuO/Li-systems. However, interpretation of the XPS spectra was ambiguous and much less clear as compared to CuO/Na as mixed oxidation states of copper were always found. This can be also taken as a hint that reactions A and B occur, which is also consistent with previous works.<sup>112</sup>

Figure 5 shows the practically obtainable capacities of CuO electrodes for lithium and sodium cells. The performance of thin film electrodes (estimate for  $q_{th,CuO}$  is 75 µAh cm<sup>-2</sup>) is further compared with conventional electrodes ( $q_{th,CuO} = 1.2$  mAh cm<sup>-2</sup> and 674 mAh g<sup>-1</sup>). Note that the theoretical capacity of sputtered thin film electrodes can only be given as a very rough estimate. On the basis of the SEM observations, we assume a perfect CuO film with a thickness of 200 nm for the calculation of  $q_{th}$ .

All electrodes show a large irreversible capacity in the first cycle, which is expected due to the initial activation of the electrode. Upon further cycling, the capacity values stabilize and decrease with increasing current. Importantly, the capacity values reach their starting values after returning to low current (0.1C). This means that no irreversible mechanical degradation took place in both lithium and sodium cells. It can be also clearly seen that the lithium cells show higher capacities. In the case of conventional electrodes, the capacities are even higher than  $q_{th}$ , which can be explained by the combination of four factors: (i) (seemingly) complete conversion of CuO to Cu, (ii) capacitive effects among the copper network that is embedded in a Li<sub>2</sub>O matrix,<sup>113–115</sup> and/or (iii) redox effects related to electrolyte decomposition, and (iv) lithium storage in carbon additive.<sup>116–121</sup> Considering (ii), Ponroux et al. showed that capacitive effects are probably negligible to the overall capacity.<sup>122</sup> Considering (iii), we never observed cell death due to drying out of our cells (neither in the case of lithium nor sodium). We, therefore, assume that continuous electrolyte decomposition, if it takes place, does not significantly contribute to the decreasing capacity values and considering (iv), the lithium storage in the carbon additive is around 20 mAh g<sup>-1</sup>. Overall, it can be concluded that, in the case of CuO/Li, reaction A takes place for the most part. In contrast, the capacities are significantly lower (~400 mAh g<sup>-1</sup>) in the case of CuO/Na. With values around 400 mAh g<sup>-1</sup>, the capacities are close to what would be expected for partial reoxidation to Cu<sub>2</sub>O only; i.e., reaction H is the dominant storage mechanism. This correlates well with the results deduced from XPS and CV measurements.

Figure 6 shows voltage profiles of CuO thin film electrodes for the 1st and 10th cycles. As expected, very large overpotentials, many steps, and a high irreversible capacity

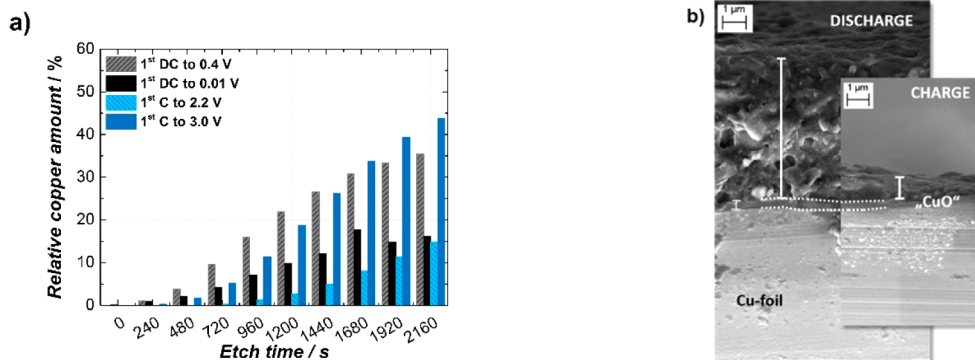


**Figure 7.** (a) The relative copper amounts calculated from the XPS depth profile in CuO/Na-system. (b) Cross-sectional SEM images of the CuO thin films after discharge and charge in the first cycle.

are found for the activation cycle due to the complex formation mechanisms of the electrode nanostructure and the surface film. In the case of sodium, the voltage profile becomes smoother upon cycling, whereas more complex mechanisms still take place in the case of lithium. The combined overpotentials are larger in the case of sodium, indicating more sluggish kinetics. Nevertheless, it should be noted that the hysteresis might also be partially thermodynamically controlled.<sup>123</sup>

**3.4.2. Surface Film Composition, SEI.** The surface film of conversion electrodes has been already studied a number of times in the case of lithium cells.<sup>116–120,124–126</sup> Only a few times, however, the SEI formation and dissolution has been studied.<sup>89,118,120,127,128</sup> To the best of our knowledge, no studies on the surface film formation of CuO electrodes in sodium cells have been reported yet.

**Initial Surface Film Formation in the First Cycle.** XPS spectra were recorded after partial discharge (0.4 V), full discharge (0.01 V), partial charge (2.2 V), and full charge (3.0 V). The copper content at these different states of discharge/charge are shown in Figure 7a and is plotted against the etching time.

Theoretically, the copper content of a CuO electrode is 50% before discharge and 25% after full discharge. Partial recharge to Cu<sub>2</sub>O amounts to a copper content of 33%. It can be seen that, in all cases, long sputtering times are needed to even approach these values and the values are significantly too small in the low potential range at 0.01 V (discharge) and 2.2 V (charge). This can only be understood with the formation and dissolution of a surface film (SEI). During discharge, a notable increase in SEI thickness occurs between 0.4 and 0.01 V. Although the copper content should increase during charging, the values are even a bit lower at 2.2 V vs Na/Na<sup>+</sup>, suggesting that the surface film has become even slightly thicker. Above this voltage, the trend is suddenly reverted, suggesting partial dissolution of the SEI. The copper content even exceeds the expected value of 33%, which might be a sign that the current collector has been reached or that preferential sputtering takes place.

Formation and partial dissolution of the SEI can be further seen from SEM images (Figure 7b) of the electrode cross section. A thick surface film of around 6 μm is found after discharge, whereas the thickness after charge is around 1 μm. Considering the thickness of the original CuO layer (200 nm), it is clear that the CuO/Na suffers from a very extensive SEI formation in the first cycle. It must be noted that the average volume expansion for oxides reaches 200% and 100% in the

cases of sodium and lithium conversion systems, respectively.<sup>15</sup> Thus, in the CuO/Na-system, the expansion due to Cu<sub>2</sub>O formation is 102.9% and another 74% during the complete reduction to Cu. Even if the expansion of the electrode only occurs vertically, the maximum thickness of a Cu + Na<sub>2</sub>O layer would be around 700 nm. Therefore, clearly, the increase in electrode thickness is dominated by surface film formation. In line with the XPS results, the SEI layer largely disappears during charging. The thickness of the remaining surface film is roughly around 1 μm. Interestingly, the surface film is much thinner in the case of lithium (see Figure 8) (the composition of the SEI is further discussed below).

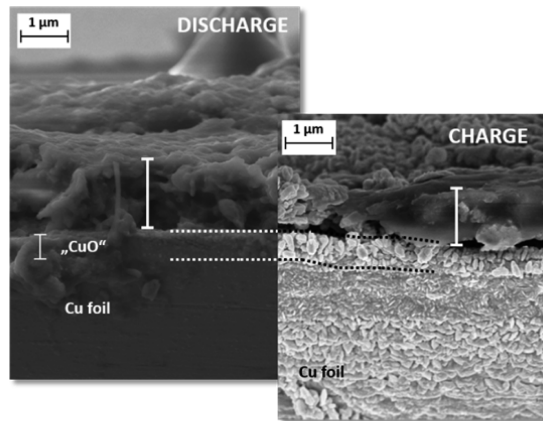


**Figure 8.** Cross-sectional SEM images of the CuO thin films after the 1<sup>st</sup> lithiation (discharge) and delithiation (charge).

**Surface Film in The 10<sup>th</sup> Cycle.** In order to determine the SEI composition, depth profiling analyses after the 10<sup>th</sup> discharge and charge had been carried out. XPS analyses of the C 1s and O 1s spectral lines are shown in Figures 9 and 10, while those corresponding to Na 1s and F 1s are shown in the Supporting Information (Figures S.I.4 and S.I.5).

C 1s spectra show that carbonates (~289 eV) are the main carbon components after both, discharge and charge processes. For the discharged state, the carbonate signal remains constant, even after prolonged etching. In contrast, hydrocarbons and small amounts of alkoxides (284.6 and 286 eV, respectively) are only detectable at the top surface of the SEI after discharge. Overall, the SEI after discharge is mostly composed of inorganic compounds, mainly carbonates, while the organic fraction decreases with depth. This overall composition agrees

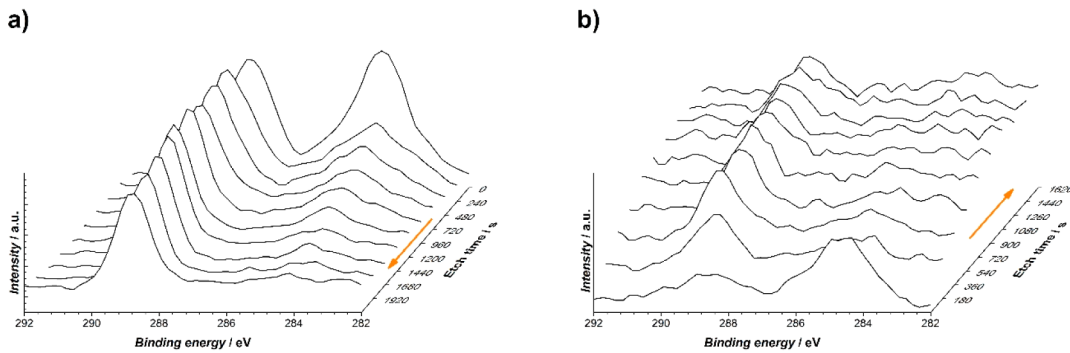


**Figure 9.** C 1s spectral line for the (a) discharged and (b) charged states in the 10th cycle as a function of time. The arrow indicates the etching progress. Axes are reversed for better visualization.

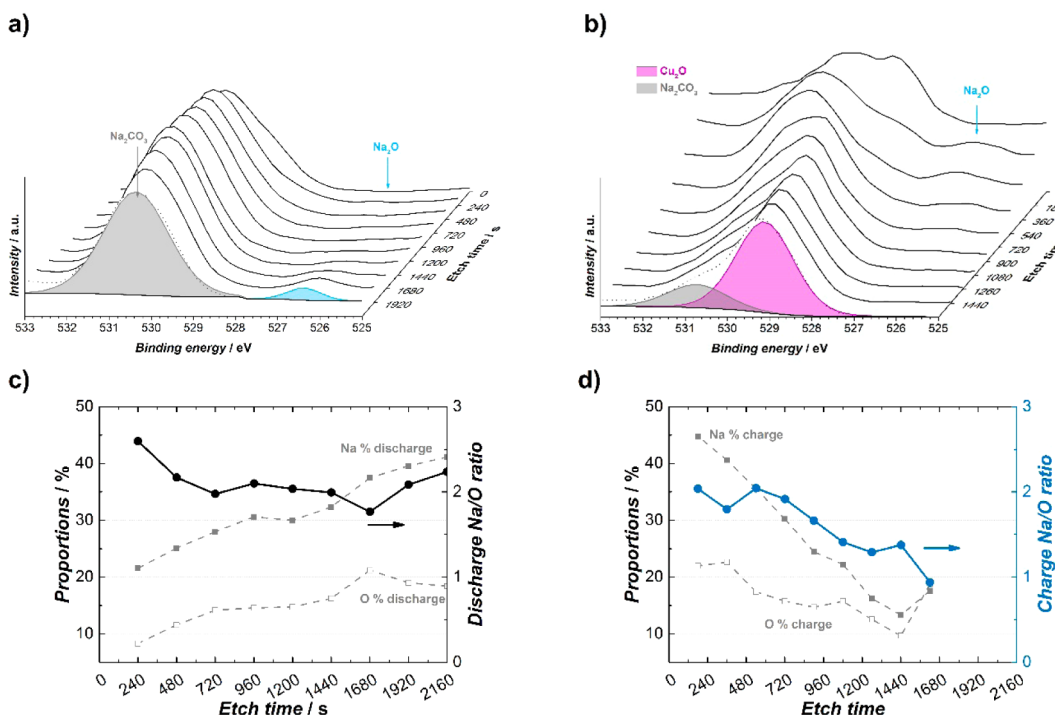


**Figure 10.** O 1s spectral line during depth profile for the (a) discharge and (b) charge state at the 10th cycle as a function of the etching time and their respective Na/O ratios (c) after discharge and (d) after charge.

with that reported previously by Komaba et al., Ponrouch et al., Muñoz-Márquez et al., and Philippe et al.<sup>90–93</sup> The residual polymer film after charge is more heterogeneous, with an outer part mainly composed of organic compounds such as hydrocarbons and an inner part mainly consisting of inorganic ones like carbonates, but also some esters (at  $\sim$ 287.9 eV). Here, we remind that, due to the absence of carbon additives in the CuO thin film electrode (excluding the unavoidable contamination of the top surface), the carbon signals can be directly ascribed to the decomposition of the electrolyte, or, more accurately, to the employed organic solvent. The overall carbonate content decreases from 52% at the end of the discharge to 17% after charge, pointing out its decomposition during charge, as previously reported in CuO/Li conversion systems by Martin et al.<sup>89</sup> Further decomposition products such as NaF are evidenced from the F 1s spectra (Figure S.I.4). Its presence is related to the decomposition of the conducting salt (NaFSI), and thus, it is homogeneously distributed (i.e.,  $\sim$ 4–5%) along the depth profile after both, discharge and charge

processes. Overall, it can be concluded that the increased thickness of the electrode mainly stems from electrolyte decomposition with  $\text{Na}_2\text{CO}_3$  and NaF being detected along the whole depth profile.

The O 1s spectra of the electrodes after discharge and charge are shown in Figure 10a,b. In order to provide further evidence about the nature of the reaction products, the Na/O ratios have been calculated after subtracting the NaF and  $\text{Na}_2\text{CO}_3$  contributions. These Na/O ratios after 10th discharge and charge are shown in Figure 10c,d.

In the case of the discharged electrode, together with the main contribution located at 530.5 eV (gray fit in Figure 10a) and associated with carbonates, especially  $\text{Na}_2\text{CO}_3$ ,<sup>92</sup> an extra contribution related to  $\text{Na}_2\text{O}$  (526.5 eV, blue fit in Figure 10a and  $\text{Na}_2\text{O}$  reference in Figure S.I.6, SI) becomes evident when increasing the etching time over 1440 s. It must be noted that this contribution emerges together with the Cu(0) in the Cu 2p region (see Figure S.I.3a, SI). However, the carbonate contribution remains constant with increasing etching time, as

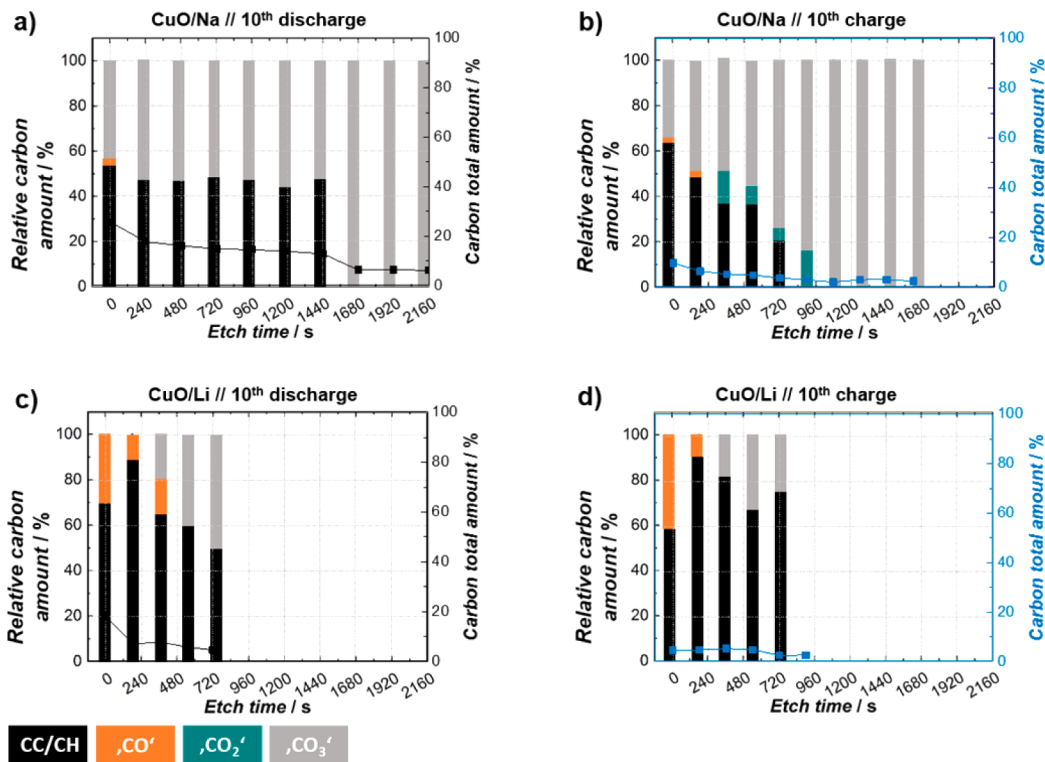
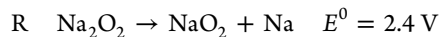
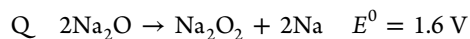
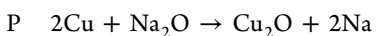


**Figure 11.** Relative carbon amount of the different carbonaceous species and total carbon amount (a) for the 10th discharge in Na- and (c) in Li-based systems and (b) for the 10th charge in Na- and (d) in Li-based systems. Hydrocarbons are denoted in black, C–O bonds in orange, C–O–O–R bonds in cyan, and carbonate species in gray.

it was shown before in the C 1s spectra. After charge, a shoulder with a binding energy at around 529.3 eV (pink fit in Figure 10b) emerges and grows with increasing etching time due to the formation of Cu<sub>2</sub>O, in good agreement with the Cu 2p spectrum after charge (see Figure S.I.3b, SI). A further O 1s contribution at 530.5 eV associated with carbonate species can also be observed. With increasing etching time, the contribution of carbonates decreases while that one related to Cu<sub>2</sub>O increases (see also the depth profiles of C 1s in Figure 9 and Cu 2p in Figure S.I.3). In addition, the small contribution around 526.5 eV representing Na<sub>2</sub>O disappears after etching for 900 s. Thus, a Na/O ratio close to 2 was attained after the discharge (see Figure 10c), while a Na/O ratio that evolves from 2 to 1 with the etching time was obtained after charge (see Figure 10d). These data further support the idea that Cu and Na<sub>2</sub>O are the discharge products, while, besides Cu<sub>2</sub>O, Na<sub>2</sub>O<sub>2</sub> is an additional charge product. In other words, elemental copper is oxidized to Cu<sub>2</sub>O during charge and additionally Na<sub>2</sub>O is partially oxidized to Na<sub>2</sub>O<sub>2</sub>. This means that, besides Cu and Na, also oxygen is redox active. We emphasize that our proof is only indirect and the following arguments speculative, but redox activity of oxygen might enable alternative reaction mechanisms. Moreover, it is worth noting that Auger peaks present in the O 1s spectra line could result in deviations from ideal Na/O ratios. Therefore, XPS analyses with a dual anode could provide more accurate evidence. In principle, the following reactions during charging can be formulated (neglecting side reactions with the surface film/electrolyte) as follows:



Reaction P is the cell reaction with Cu<sub>2</sub>O as charge product. If oxygen becomes redox active and overpotentials for reaction P are large, reaction Q might independently take place with the result of forming Na<sub>2</sub>O<sub>2</sub>. In principle, the formed Na<sub>2</sub>O<sub>2</sub> can further react to form Cu<sub>2</sub>O or CuO (see reactions J and K). If Na<sub>2</sub>O<sub>2</sub> is inactive, the full oxidation of Cu to CuO is intrinsically limited. Reaction R is unlikely (no proof for NaO<sub>2</sub> formation). Clearly, redox activity of oxygen would add to the already complex and poorly understood reaction mechanisms of conversion electrodes. Several reactions might simultaneously compete. Such a behavior would also provide additional arguments to understand whether the origin of the voltage hysteresis is purely kinetic or also due to thermodynamics. Clearly, more insight is needed. A more thorough analysis of the electrode compositions at different states of discharge and charge has to be part of future studies.

**3.4.3. Surface Films of CuO/Na and CuO/Li in Comparison.** Finally, the SEI after the 10th discharge and charge of both CuO/alkali-systems have been compared. For this purpose, the proportions of each carbon species and the total carbon amount have been plotted vs the etching time in Figure 11. The discharged and charged states are shown in black and blue, respectively, while the different carbonaceous species (hydrocarbons in black, alkoxides in orange, esters in cyan, and carbonates in gray) are displayed in the histogram.

Carbon contributions are found within the whole depth profile of CuO/Na half-cells (Figure 11a,b) after both, discharge and charge processes. In contrast, in the analogous Li-systems, carbon contributions disappear after etching for 720

s, as expected from the thicker dimensions of the SEI in the CuO/Na-based systems ( $\sim 6 \mu\text{m}$  vs  $1.5 \mu\text{m}$ ). These results are in good agreement with previous studies on  $\text{Fe}_2\text{O}_3$  conversion systems,<sup>93</sup> although, the thicknesses of the SEIs might have been underestimated for both, sodium-based anode materials and CuO/Li-systems.<sup>89,91,92</sup>

After discharge, the SEI in the CuO/Na-based system is mainly composed of homogeneously distributed inorganic products, such as carbonates, derived from the electrolyte decomposition. In contrast, the SEI of CuO/Li-systems is mainly organic, and mostly composed from hydrocarbons. Their contribution decreases with increasing the sputter time. In turn, the carbonate contribution increases simultaneously. Hence, for CuO/Li, a layer-like SEI, with a more organic outer part and a more inorganic inner part, is progressively formed which significantly differs from what is found in the case of CuO/Na. These results are supported by the cross-sectional SEM images presented in Figure 8. Although also being quite thick, the surface film after discharge is much thinner as compared to sodium (see Figure 7b).

The dynamic formation and decomposition of the surface film on CuO thin films is schematically shown in Figure 12. In

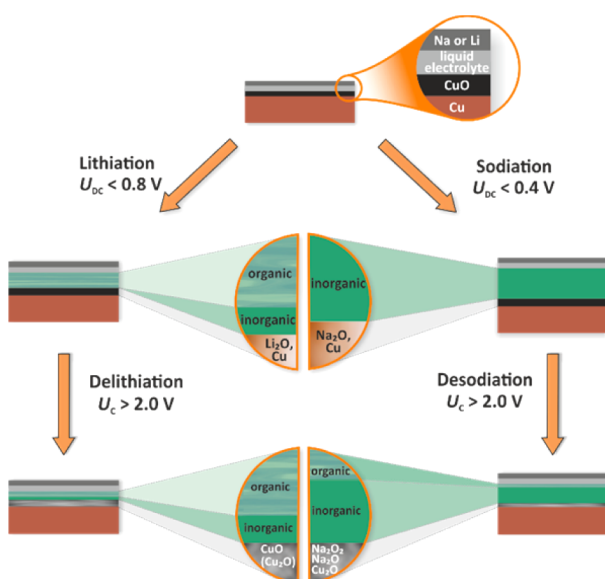


**Figure 12.** Schematic model for SEI evolution and composition in CuO/Na- and CuO/Li-systems.

the case of sodium, the SEI is much thicker as compared to lithium. The SEI forms during discharge, especially at potentials below  $0.4 \text{ V}$  vs  $\text{Na}/\text{Na}^+$  and partially decomposes during charge ( $> 2.2 \text{ V}$  vs  $\text{Na}/\text{Na}^+$ ). Furthermore, its composition is more heterogeneous and mainly formed by inorganic constituents.

#### 4. CONCLUSION

The conversion reaction of CuO thin films with sodium has been studied. Well-defined and additive-free thin films were chosen as model electrodes to study the reaction mechanism and surface film formation. Electrodes were studied during the 1st cycle (activation cycle) and the 10th cycle (stabilized state). Considering the electrode reaction, it was found that the CuO/Na-system is only partly reversible. The discharge products are Cu and  $\text{Na}_2\text{O}$ , whereas the charge product is  $\text{Cu}_2\text{O}$ . This is in contrast to the CuO/Li-system, where at least partially CuO

reforms during charging. Moreover, it seems that, besides sodium and copper, also oxygen is redox active and  $\text{Na}_2\text{O}_2$  forms during charging. The possible appearance of  $\text{Na}_2\text{O}_2$  might also help to explain the origin of the voltage hysteresis that is considered to be determined by kinetics and thermodynamics.

Morphology and chemical composition of the surface films were studied by SEM and XPS. Surface film formation during the first sodiation/lithiation was observed with thickness and chemical composition depending on the alkali metal. For sodium, a very thick SEI (approximately  $6 \mu\text{m}$ !) formed during discharge. The overall composition is fairly homogeneous and inorganic in nature ( $\text{Na}_2\text{CO}_3$  and  $\text{NaF}$ ). For lithium, the SEI is around  $1 \mu\text{m}$  thick, structurally more heterogeneous and more organic. During charging, the SEI largely decomposes in the case of CuO/Na and the remaining surface film thickness is around  $1 \mu\text{m}$ . Overall, this study demonstrated that the reaction mechanism and surface film formation of conversion electrodes are strongly influenced by the size of the alkali ion. Only few aspects could be clarified so far, but there is clearly a lot to be discovered. Understanding how the size of the alkali ion influences kinetics (diffusion, charge transfer, etc.) and thermodynamics (phase stability) as well as surface film formation is a challenging, but worthwhile, scientific goal. With respect to application, one might hope that some well-known challenges for conversion reactions can be overcome by replacing lithium by sodium; however, no improvement has been demonstrated so far for the here discussed CuO compound as well as for other conversion materials. More systematic studies are needed to clarify the potential for application.

#### ■ ASSOCIATED CONTENT

##### S Supporting Information

The Supporting Information is available free of charge on the ACS Publications website at DOI: [10.1021/acs.jpcc.5b10642](https://doi.org/10.1021/acs.jpcc.5b10642).

Cycle performance of bulk CuO/Na-systems; cross section of the CuO thin film electrode; Cu 2p, F 1s, and Na 1s spectral lines during depth profile; and XPS depth profiles (PDF)

#### ■ AUTHOR INFORMATION

##### Corresponding Author

\*E-mail: philipp.adelhelm@uni-jena.de.

##### Notes

The authors declare no competing financial interest.

#### ■ ACKNOWLEDGMENTS

Financial support is gratefully acknowledged from the German Research Foundation (DFG) within the project “Thermodynamik und Kinetik von Konversionsreaktionen in neuen, natriumbasierten Batteriesystemen”, the state of Hesse (Landes-Offensive zur Entwicklung Wissenschaftlich-ökonomischer Exzellenz - LOEWE) within the project Store-E (Stoffspeicherung in Grenzflächen). We thank Dr. Luerßen for helpful discussions on data treatment and interpretation. P.A. acknowledges support from the Federal state of Thuringia within the ProExzellenz program.

#### ■ REFERENCES

- (1) Adelhelm, P.; Hartmann, P.; Bender, C. L.; Busche, M.; Eufinger, C.; Janek, J. From Lithium to Sodium: Cell Chemistry of Room

- Temperature Sodium–air and Sodium–sulfur Batteries. *Beilstein J. Nanotechnol.* **2015**, *6*, 1016–1055.
- (2) Poizot, P.; Laruelle, S.; Gruegeon, S.; Dupont, L.; Tarascon, J.-M. Nano-Sizedtransition-Metaloxides as Negative-Electrode Materials for Lithium-Ion Batteries. *Nature* **2000**, *407*, 496–499.
  - (3) Cabana, J.; Monconduit, L.; Larcher, D.; Palacín, M. R. Beyond Intercalation-Based Li-Ion Batteries: The State of the Art and Challenges of Electrode Materials Reacting through Conversion Reactions. *Adv. Mater.* **2010**, *22* (35), E170–E192.
  - (4) Yabuuchi, N.; Kubota, K.; Dahbi, M.; Komaba, S. Research Development on Sodium-Ion Batteries. *Chem. Rev.* **2014**, *114* (23), 11636–11682.
  - (5) Riedel, E.; Janiak, C. *Anorganische Chemie*; De Gruyter: Berlin, 2011.
  - (6) Kim, S.-W.; Seo, D.-H.; Ma, X.; Ceder, G.; Kang, K. Electrode Materials for Rechargeable Sodium-Ion Batteries: Potential Alternatives to Current Lithium-Ion Batteries. *Adv. Energy Mater.* **2012**, *2* (7), 710–721.
  - (7) Ellis, B. L.; Nazar, L. F. Sodium and Sodium-Ion Energy Storage Batteries. *Curr. Opin. Solid State Mater. Sci.* **2012**, *16* (4), 168–177.
  - (8) Palomares, V.; Casas-Cabanas, M.; Castillo-Martinez, E.; Han, M. H.; Rojo, T. Update on Na-Based Battery Materials. A Growing Research Path. *Energy Environ. Sci.* **2013**, *6*, 2312–2337.
  - (9) Ha, S.; Kim, J.-K.; Choi, A.; Kim, Y.; Lee, K. T. Sodium-Metal Halide and Sodium-Air Batteries. *ChemPhysChem* **2014**, *15* (10), 1971–1982.
  - (10) Kim, Y.; Ha, K.-H.; Oh, S. M.; Lee, K. T. High-Capacity Anode Materials for Sodium-Ion Batteries. *Chem. - Eur. J.* **2014**, *20* (38), 11980–11992.
  - (11) Wang, L. P.; Yu, L.; Wang, X.; Srinivasan, M.; Xu, Z. J. Recent Developments in Electrode Materials for Sodium-Ion Batteries. *J. Mater. Chem. A* **2015**, *3* (18), 9353–9378.
  - (12) Sawicki, M.; Shaw, L. L. Advances and Challenges of Sodium Ion Batteries as Post Lithium Ion Batteries. *RSC Adv.* **2015**, *5* (65), 53129–53154.
  - (13) Kundu, D.; Talaie, E.; Duffort, V.; Nazar, L. F. The Emerging Chemistry of Sodium Ion Batteries for Electrochemical Energy Storage. *Angew. Chem., Int. Ed.* **2015**, *54* (11), 3431–3448.
  - (14) Bommier, C.; Ji, X. Recent Development on Anodes for Na-Ion Batteries. *Isr. J. Chem.* **2015**, *55* (5), 486–507.
  - (15) Klein, F.; Jache, B.; Bhide, A.; Adelhelm, P. Conversion Reactions for Sodium-Ion Batteries. *Phys. Chem. Chem. Phys.* **2013**, *15* (38), 15876–15887.
  - (16) Malini, R.; Uma, U.; Sheela, T.; Ganeshan, M.; Renganathan, N. G. Conversion Reactions: A New Pathway to Realise Energy in Lithium-Ion Battery—review. *Ionics* **2009**, *15* (3), 301–307.
  - (17) Hasa, I.; Verrelli, R.; Hassoun, J. Transition Metal Oxide-Carbon Composites as Conversion Anodes for Sodium-Ion Battery. *Electrochim. Acta* **2015**, *173*, 613–618.
  - (18) Liu, H.; Cao, F.; Zheng, H.; Sheng, H.; Li, L.; Wu, S.; Liu, C.; Wang, J. In Situ Observation of the Sodiation Process in CuO Nanowires. *Chem. Commun.* **2015**, *51* (52), 10443–10446.
  - (19) Lu, Y.; Zhang, N.; Zhao, Q.; Liang, J.; Chen, J. Micro-Nanostructured CuO/C Spheres as High-Performance Anode Materials for Na-Ion Batteries. *Nanoscale* **2015**, *7* (6), 2770–2276.
  - (20) Yuan, S.; Huang, X.; Ma, D.; Wang, H.; Meng, F.; Zhang, X. Engraving Copper Foil to Give Large-Scale Binder-Free Porous CuO Arrays for a High-Performance Sodium-Ion Battery anode. *Adv. Mater.* **2014**, *26* (14), 2273–2279.
  - (21) Li, X.; Hector, A. L.; Owen, J. R. Evaluation of Cu<sub>3</sub>N and CuO as Negative Electrode Materials for Sodium Batteries. *J. Phys. Chem. C* **2014**, *118*, 29568–29573.
  - (22) Wang, L.; Zhang, K.; Hu, Z.; Duan, W.; Cheng, F.; Chen, J. Porous CuO Nanowires as the Anode of Rechargeable Na-Ion Batteries. *Nano Res.* **2014**, *7* (2), 199–208.
  - (23) Liu, Y.; Qiao, Y.; Zhang, W.; Hu, P.; Chen, C.; Li, Z.; Yuan, L.; Hu, X.; Huang, Y. Facile Fabrication of CuO Nanosheets on Cu Substrate as Anode Materials for Electrochemical Energy Storage. *J. Alloys Compd.* **2014**, *586*, 208–215.
  - (24) Jian, Z.; Liu, P.; Li, F.; Chen, M.; Zhou, H. Monodispersed Hierarchical Co<sub>3</sub>O<sub>4</sub> Spheres Intertwined with Carbon Nanotubes for Use as Anode Materials in Sodium-Ion Batteries. *J. Mater. Chem. A* **2014**, *2* (34), 13805–13809.
  - (25) Liu, Y.; Cheng, Z.; Sun, H.; Arandiyani, H.; Li, J.; Ahmad, M. Mesoporous Co<sub>3</sub>O<sub>4</sub> sheets/3D Graphene Networks Nanohybrids for High-Performance Sodium-Ion Battery Anode. *J. Power Sources* **2015**, *273*, 878–884.
  - (26) Wen, J.-W.; Zhang, D.-W.; Zang, Y.; Sun, X.; Cheng, B.; Ding, C.-X.; Yu, Y.; Chen, C.-H. Li and Na Storage Behavior of Bowl-like Hollow Co<sub>3</sub>O<sub>4</sub> Microspheres as an Anode Material for Lithium-Ion and Sodium-Ion Batteries. *Electrochim. Acta* **2014**, *132*, 193–199.
  - (27) Klavetter, K. C.; Garcia, S.; Dahal, N.; Snider, J. L.; Pedro de Souza, J.; Cell, T. H.; Cassara, M. A.; Heller, A.; Humphrey, S. M.; Mullins, C. B. Li- and Na-Reduction Products of Meso-Co<sub>3</sub>O<sub>4</sub> Form High-Rate, Stably Cycling Battery Anode Materials. *J. Mater. Chem. A* **2014**, *2* (34), 14209–14221.
  - (28) Sun, W.; Rui, X.; Zhu, J.; Yu, L.; Zhang, Y.; Xu, Z.; Madhavi, S.; Yan, Q. Ultrathin Nickel Oxide Nanosheets for Enhanced Sodium and Lithium Storage. *J. Power Sources* **2015**, *274*, 755–761.
  - (29) Oh, S.; Myung, S.; Yoon, C. S.; Lu, J.; Hassoun, J.; Scrosati, B.; Amine, K.; Sun, Y. Advanced Na[Ni<sub>0.25</sub>Fe<sub>0.5</sub>Mn<sub>0.25</sub>]O<sub>2</sub>/C-Fe<sub>3</sub>O<sub>4</sub> Sodium-Ion Batteries Using EMS Electrolyte for Energy Storage. *Nano Lett.* **2014**, *14*, 1620–1626.
  - (30) Zhang, S.; Li, W.; Tan, B.; Chou, S.; Li, Z.; Dou, S. One-Pot Synthesis of Ultra-Small Magnetite Nanoparticles on the Surface of Reduced Graphene Oxide Nanosheets as Anodes for Sodium-Ion Batteries. *J. Mater. Chem. A* **2015**, *3* (9), 4793–4798.
  - (31) Park, D.; Myung, S. Carbon-Coated Magnetite Embedded on Carbon Nanotubes for Rechargeable Lithium and Sodium Batteries. *ACS Appl. Mater. Interfaces* **2014**, *6*, 11749–11757.
  - (32) Hariharan, S.; Saravanan, K.; Ramar, V.; Balaya, P. A Rationally Designed Dual Role Anode Material for Lithium-Ion and Sodium-Ion Batteries: Case Study of Eco-Friendly Fe<sub>3</sub>O<sub>4</sub>. *Phys. Chem. Chem. Phys.* **2013**, *15* (8), 2945–2953.
  - (33) Liu, X.; Chen, T.; Chu, H.; Niu, L.; Sun, Z.; Pan, L.; Sun, C. Q. Fe<sub>2</sub>O<sub>3</sub>-Reduced Graphene Oxide Composites Synthesized via Microwave-Assisted Method for Sodium Ion Batteries. *Electrochim. Acta* **2015**, *166*, 12–16.
  - (34) Wu, Z.; Zhong, Y.; Liu, J.; Wu, J.; Guo, X.; Zhong, B.; Zhang, Z. Subunits Controlled Synthesis of α-Fe<sub>2</sub>O<sub>3</sub> Multi-Shelled Core–shell Microspheres and Their Effects on Lithium/sodium Ion Battery Performances. *J. Mater. Chem. A* **2015**, *3*, 10092–10099.
  - (35) Zhang, Z.-J.; Wang, Y.-X.; Chou, S.-L.; Li, H.-J.; Liu, H.-K.; Wang, J.-Z. Rapid Synthesis of α-Fe<sub>2</sub>O<sub>3</sub>/rGO Nanocomposites by Microwave Autoclave as Superior Anodes for Sodium-Ion Batteries. *J. Power Sources* **2015**, *280*, 107–113.
  - (36) Jian, Z.; Zhao, B.; Liu, P.; Li, F.; Zheng, M.; Chen, M.; Shi, Y.; Zhou, H. Fe<sub>2</sub>O<sub>3</sub> Nanocrystals Anchored onto Graphene Nanosheets as the Anode Material for Low-Cost Sodium-Ion Batteries. *Chem. Commun.* **2014**, *50* (10), 1215–1217.
  - (37) Huang, B.; Tai, K.; Zhang, M.; Xiao, Y.; Dillon, S. J. Comparative Study of Li and Na Electrochemical Reactions with Iron Oxide Nanowires. *Electrochim. Acta* **2014**, *118*, 143–149.
  - (38) Zhao, Y.; Feng, Z.; Xu, Z. J. Yolk-Shell Fe<sub>2</sub>O<sub>3</sub>OC Composites Anchored on MWNTs with Enhanced Lithium and Sodium Storage. *Nanoscale* **2015**, *7* (21), 9520–9525.
  - (39) Sun, B.; Bao, S. J.; Le Xie, J.; Li, C. M. Vacuum-Annealing-Tailored Robust and Flexible Nanopore-Structured γ-Fe<sub>2</sub>O<sub>3</sub> Film Anodes for High Capacity and Long Life Na-Ion Batteries. *RSC Adv.* **2014**, *4* (69), 36815–36820.
  - (40) Nageswara Rao, B.; Ramesh Kumar, P.; Padmaraj, O.; Venkateswarlu, M.; Satyanarayana, N. Rapid Microwave Assisted Hydrothermal Synthesis of Porous α-Fe<sub>2</sub>O<sub>3</sub> Nanostructures as Stable and High Capacity Negative Electrode for Lithium and Sodium Ion Batteries. *RSC Adv.* **2015**, *5* (44), 34761–34768.
  - (41) Valvo, M.; Lindgren, F.; Lafont, U.; Björefors, F.; Edström, K. Towards More Sustainable Negative Electrodes in Na-Ion Batteries via Nanostructured Iron Oxide. *J. Power Sources* **2014**, *245*, 967–978.

- (42) Hariharan, S.; Saravanan, K.; Balaya, P.  $\alpha$ -MoO<sub>3</sub>: A High Performance Anode Material for Sodium-Ion Batteries. *Electrochim. Commun.* **2013**, *31*, 5–9.
- (43) Choi, S. H.; Kang, Y. C. Sodium Ion Storage Properties of WS<sub>2</sub>-Decorated Three-Dimensional Reduced Graphene Oxide Microspheres. *Nanoscale* **2015**, *7* (9), 3965–3970.
- (44) Shadik, Z.; Cao, M.-H.; Ding, F.; Sang, L.; Fu, Z.-W. Improved Electrochemical Performance of CoS<sub>2</sub>-MWCNT Nanocomposites for Sodium-Ion Batteries. *Chem. Commun.* **2015**, *51* (52), 10486–10489.
- (45) Du, Y.; Zhu, X.; Zhou, X.; Hu, L.; Dai, Z.; Bao, J. Co<sub>3</sub>S<sub>4</sub> Porous Nanosheets Embedded in Graphene Sheets as High-Performance Anode Materials for Lithium and Sodium Storage. *J. Mater. Chem. A* **2015**, *3* (13), 6787–6791.
- (46) Walter, M.; Zünd, T.; Kovalenko, M. V. Pyrite (FeS<sub>2</sub>) Nanocrystals as Inexpensive High-Performance Lithium-Ion Cathode and Sodium-Ion Anode Materials. *Nanoscale* **2015**, *7* (20), 9158–9163.
- (47) Zhu, Y.; Suo, L.; Gao, T.; Fan, X.; Han, F.; Wang, C. Ether-Based Electrolyte Enabled Na/FeS<sub>2</sub> Rechargeable Batteries. *Electrochim. Commun.* **2015**, *54*, 18–22.
- (48) Kitajou, A.; Yamaguchi, J.; Hara, S.; Okada, S. Discharge/charge Reaction Mechanism of a Pyrite-Type FeS<sub>2</sub> Cathode for Sodium Secondary Batteries. *J. Power Sources* **2014**, *247*, 391–395.
- (49) Su, D.; Dou, S.; Wang, G. WS<sub>2</sub>@graphene Nanocomposites as Anode Materials for Na-Ion Batteries with Enhanced Electrochemical Performances. *Chem. Commun.* **2014**, *50* (32), 4192–4195.
- (50) Xu, M.; Yi, F.; Niu, Y.; Xie, J.; Hou, J.; Liu, S.; Hu, W.; Li, Y.; Li, C. M. Solvent-Mediated Directionally Self-Assembling MoS<sub>2</sub> Nanosheets into a Novel Worm-like Structure and Its Application in Sodium Batteries. *J. Mater. Chem. A* **2015**, *3* (18), 9932–9937.
- (51) Xiong, X.; Luo, W.; Hu, X.; Chen, C.; Qie, L.; Hou, D.; Huang, Y. Flexible Membranes of MoS<sub>2</sub>/C Nanofibers by Electrospinning as Binder-Free Anodes for High-Performance Sodium-Ion Batteries. *Sci. Rep.* **2015**, *5*, 9254.
- (52) Zhao, L.; Qi, L.; Wang, H. MoS<sub>2</sub> – C/graphite, an Electric Energy Storage Device Using Na<sup>+</sup>-Based Organic Electrolytes. *RSC Adv.* **2015**, *5* (20), 15431–15437.
- (53) Lacey, S. D.; Wan, J.; Cresce, A. V. W.; Russell, S. M.; Dai, J.; Bao, W.; Xu, K.; Hu, L. Atomic Force Microscopy Studies on Molybdenum Disulfide Flakes as Sodium-Ion Anodes. *Nano Lett.* **2015**, *15*, 1018–1024.
- (54) Wang, J.; Luo, C.; Gao, T.; Langrock, A.; Mignerey, A. C.; Wang, C. An Advanced MoS<sub>2</sub>/carbon Anode for High-Performance Sodium-Ion Batteries. *Small* **2015**, *11* (4), 473–481.
- (55) Qin, W.; Chen, T.; Pan, L.; Niu, L.; Hu, B.; Li, D.; Li, J.; Sun, Z. MoS<sub>2</sub>-Reduced Graphene Oxide Composites via Microwave Assisted Synthesis for Sodium Ion Battery Anode with Improved Capacity and Cycling Performance. *Electrochim. Acta* **2015**, *153*, 55–61.
- (56) Xie, X.; Ao, Z.; Su, D.; Zhang, J.; Wang, G. MoS<sub>2</sub>/Graphene Composite Anodes with Enhanced Performance for Sodium-Ion Batteries: The Role of the Two-Dimensional Heterointerface. *Adv. Funct. Mater.* **2015**, *25* (9), 1393–1403.
- (57) Zhang, S.; Yu, X.; Yu, H.; Chen, Y.; Gao, P.; Li, C.; Zhu, C. Growth of Ultrathin MoS<sub>2</sub> Nanosheets with Expanded Spacing of (002) Plane on Carbon Nanotubes for High-Performance Sodium-Ion Battery Anodes. *ACS Appl. Mater. Interfaces* **2014**, *6*, 21880–21885.
- (58) Hu, Z.; Wang, L.; Zhang, K.; Wang, J.; Cheng, F.; Tao, Z.; Chen, J. MoS<sub>2</sub> Nanoflowers with Expanded Interlayers as High-Performance Anodes for Sodium-Ion Batteries. *Angew. Chem., Int. Ed.* **2014**, *53* (47), 12794–12798.
- (59) Zhu, C.; Mu, X.; van Aken, P. A.; Yu, Y.; Maier, J. Single-Layered Ultrasmall Nanoplates of MoS<sub>2</sub> Embedded in Carbon Nanofibers with Excellent Electrochemical Performance for Lithium and Sodium Storage. *Angew. Chem., Int. Ed.* **2014**, *53* (8), 2152–2156.
- (60) Wang, Y.-X.; Seng, K. H.; Chou, S.-L.; Wang, J.-Z.; Guo, Z.; Wexler, D.; Liu, H.-K.; Dou, S.-X. Reversible Sodium Storage via Conversion Reaction of a MoS<sub>2</sub>-C Composite. *Chem. Commun.* **2014**, *50* (73), 10730–10733.
- (61) Shang, C.; Dong, S.; Zhang, S.; Hu, P.; Zhang, C.; Cui, G. A Ni<sub>3</sub>S<sub>2</sub>-PEDOT Monolithic Electrode for Sodium Batteries. *Electrochim. Commun.* **2015**, *50*, 24–27.
- (62) Ryu, H.-S.; Kim, J.-S.; Park, J.; Park, J.-Y.; Cho, G.-B.; Liu, X.; Ahn, I.-S.; Kim, K.-W.; Ahn, J.-H.; Ahn, J.-P.; et al. Degradation Mechanism of Room Temperature Na/Ni<sub>3</sub>S<sub>2</sub> Cells Using Ni<sub>3</sub>S<sub>2</sub> Electrodes Prepared by Mechanical Alloying. *J. Power Sources* **2013**, *244*, 764–770.
- (63) Kim, J.-S.; Ahn, H.-J.; Ryu, H.-S.; Kim, D.-J.; Cho, G.-B.; Kim, K.-W.; Nam, T.-H.; Ahn, J. H. The Discharge Properties of Na/Ni<sub>3</sub>S<sub>2</sub> Cell at Ambient Temperature. *J. Power Sources* **2008**, *178* (2), 852–856.
- (64) Liu, X.; Kang, S.; Kim, J.; Ahn, H.; Lim, S.; Ahn, I. A Study of Ni<sub>3</sub>S<sub>2</sub> Synthesized by Mechanical Alloying for Na/Ni<sub>3</sub>S<sub>2</sub> Cell. *Rare Met.* **2011**, *30* (S1), 5–10.
- (65) Kim, J.-S.; Kim, D.-Y.; Cho, G.-B.; Nam, T.-H.; Kim, K.-W.; Ryu, H.-S.; Ahn, J.-H.; Ahn, H.-J. The Electrochemical Properties of Copper Sulfide as Cathode Material for Rechargeable Sodium Cell at Room Temperature. *J. Power Sources* **2009**, *189* (1), 864–868.
- (66) Tan, J.; Liu, L.; Guo, S.; Hu, H.; Yan, Z.; Zhou, Q.; Huang, Z.; Shu, H.; Yang, X.; Wang, X. The Electrochemical Performance and Mechanism of Cobalt(II)Fluoride as Anode Material for Lithium and Sodium Ion Batteries. *Electrochim. Acta* **2015**, *168*, 225–233.
- (67) Fullenwarth, J.; Darwiche, A.; Soares, A.; Donnadieu, B.; Monconduit, L. NiP<sub>3</sub>: A Promising Negative Electrode for Li- and Na-Ion Batteries. *J. Mater. Chem. A* **2014**, *2* (7), 2050.
- (68) Cui, Z.; Li, C.; Yu, P.; Yang, M.; Guo, X.; Yin, C. Reaction Pathway and Wiring Network Dependent Li/Na Storage of Micro-Sized Conversion Anode with Mesoporosity and Metallic Conductivity. *J. Mater. Chem. A* **2015**, *3* (2), 509–514.
- (69) Li, X.; Hasan, M. M.; Hector, A. L.; Owen, J. R. Performance of Nanocrystalline Ni<sub>3</sub>N as a Negative Electrode for Sodium-Ion Batteries. *J. Mater. Chem. A* **2013**, *1* (21), 6441–6445.
- (70) Chen, G.-Y.; Sun, Q.; Yue, J.-L.; Shadik, Z.; Yang, Y.; Ding, F.; Sang, L.; Fu, Z.-W. Conversion and Displacement Reaction Types of Transition Metal Compounds for Sodium Ion Battery. *J. Power Sources* **2015**, *284*, 115–121.
- (71) Wang, H.; Lan, X.; Jiang, D.; Zhang, Y.; Zhong, H.; Zhang, Z.; Jiang, Y. Sodium Storage and Transport Properties in Pyrolysis Synthesized MoS<sub>2</sub> Nanoplates for High Performance Sodium-Ion Batteries. *J. Power Sources* **2015**, *283*, 187–194.
- (72) Yue, J.-L.; Sun, Q.; Fu, Z.-W. Cu<sub>2</sub>Se with Facile Synthesis as a Cathode Material for Rechargeable Sodium Batteries. *Chem. Commun.* **2013**, *49* (52), 5868–5870.
- (73) Krenzel, M.; Adelhelm, P.; Klein, F.; Bensch, W. FeV<sub>2</sub>S<sub>4</sub> as a High Capacity Electrode Material for Sodium-Ion Batteries. *Chem. Commun.* **2015**, *51*, 13500–13503.
- (74) Choi, S. H.; Kang, Y. C. Synergetic Compositional and Morphological Effects for Improved Na<sup>+</sup> Storage Properties of Ni<sub>3</sub>Co<sub>6</sub>S<sub>8</sub>-Reduced Graphene Oxide Composite Powders. *Nanoscale* **2015**, *7* (14), 6230–6237.
- (75) Brown, Z. L.; Smith, S.; Obrovac, M. N. Mixed Transition Metal Titanate and Vanadate Negative Electrode Materials for Na-Ion Batteries. *J. Electrochim. Soc.* **2015**, *162* (1), A15–A20.
- (76) Alcántara, R.; Jaraba, M.; Lavela, P.; Tirado, J. L. NiCo<sub>2</sub>O<sub>4</sub> Spinel: First Report on a Transition Metal Oxide for the Negative Electrode of Sodium-Ion Batteries. *Chem. Mater.* **2002**, *14* (7), 2847–2848.
- (77) He, K.; Lin, F.; Zhu, Y.; Yu, X.; Li, J.; Lin, R.; Nordlund, D.; Weng, T.-C.; Richards, R. M.; Yang, X.-Q.; et al. Sodiation Kinetics of Metal Oxide Conversion Electrodes: A Comparative Study with Lithiation. *Nano Lett.* **2015**, *15* (9), 5755–5763.
- (78) Débart, A.; Dupont, L.; Poizot, P.; Leriche, J.-B.; Tarascon, J. M. A Transmission Electron Microscopy Study of the Reactivity Mechanism of Tailor-Made CuO Particles toward Lithium. *J. Electrochim. Soc.* **2001**, *148* (11), A1266–A1274.
- (79) Jumel, Y.; Lambin, O.; Brousseley, M. Spirally Wound Lithium Cupric Oxide Organic Electrolyte Cells. In *Proceedings of the*

- Symposium on Lithium Batteries, Washington, DC, 1983; Electrochemical Society: Pennington, NJ, 1984; pp 293–300.
- (80) Podhájeký, P.; Klápste, B.; Novák, P.; Mrha, J.; Moshtev, R.; Manev, V.; Nassalevska, A. The Influence of Preparation Conditions on the Electrochemical Behaviour of CuO in a Li/CuO Cell. *J. Power Sources* **1985**, *14*, 269–275.
- (81) Podhájeký, P.; Scrosati, B. Copper Oxide Cathodes for Lithium Organic Electrolyte Batteries. *J. Power Sources* **1985**, *16*, 309–317.
- (82) Novák, P. CuO Cathode in Lithium Cells-II.\*Reduction Mechanism of CuO. *Electrochim. Acta* **1985**, *30* (7), 1687–1692.
- (83) Novák, P. CuO Cathode in Lithium Cells - III. Its Discharge Kinetics. *Electrochim. Acta* **1986**, *31* (9), 1167–1173.
- (84) Godshall, N. A. Lithium Transport in Ternary Lithium-Copper-Oxygen Cathode Materials. *Solid State Ionics* **1986**, *18–19*, 788–793.
- (85) Hibble, S. J.; Malatesta, C.; Dickens, P. G. The Chemical and Electrochemical Lithiation of CuO: An Analytical, Electron Microscopy Investigation. *Solid State Ionics* **1990**, *39*, 289–295.
- (86) Meyer, B. K.; Polity, A.; Reppin, D.; Becker, M.; Hering, P.; Klar, P. J.; Sander, T.; Reindl, C.; Benz, J.; Eickhoff, M.; et al. Binary Copper Oxide Semiconductors: From Materials towards Devices. *Phys. Status Solidi B* **2012**, *249* (8), 1487–1509.
- (87) Heinemann, M.; Eifert, B.; Heiliger, C. Band Structure and Phase Stability of the Copper Oxides Cu<sub>2</sub>O, CuO, and Cu<sub>4</sub>O<sub>3</sub>. *Phys. Rev. B: Condens. Matter Mater. Phys.* **2013**, *87* (11), 115111–115115.
- (88) Martin, L.; Martinez, H.; Poinot, D.; Pecquenard, B.; Le Cras, F. Comprehensive X-Ray Photoelectron Spectroscopy Study of the Conversion Reaction Mechanism of CuO in Lithiated Thin Film Electrodes. *J. Phys. Chem. C* **2013**, *117*, 4421–4430.
- (89) Martin, L.; Martinez, H.; Poinot, D.; Pecquenard, B.; Le Cras, F. Direct Observation of Important Morphology and Composition Changes at the Surface of the CuO Conversion Material in Lithium Batteries. *J. Power Sources* **2014**, *248*, 861–873.
- (90) Komaba, S.; Murata, W.; Ishikawa, T.; Yabuuchi, N.; Ozeki, T.; Nakayama, T.; Ogata, A.; Gotoh, K.; Fujiwara, K. Electrochemical Na Insertion and Solid Electrolyte Interphase for Hard-Carbon Electrodes and Application to Na-Ion Batteries. *Adv. Funct. Mater.* **2011**, *21* (20), 3859–3867.
- (91) Ponrouch, A.; Dedryvère, R.; Monti, D.; Demet, A. E.; Mba, J. M. A.; Croguennec, L.; Masquelier, C.; Johansson, P.; Palacin, M. R. Towards High Energy Density Sodium Ion Batteries through Electrolyte Optimization. *Energy Environ. Sci.* **2013**, *6*, 2361–2369.
- (92) Muñoz-Márquez, M. A.; Zarrabeitia, M.; Castillo-Martínez, E.; Eguía-Barrio, A.; Rojo, T.; Casas-Cabanas, M. Composition and Evolution of the Solid-Electrolyte Interphase in Na<sub>2</sub>Ti<sub>3</sub>O<sub>7</sub> Electrodes for Na-Ion Batteries: XPS and Auger Parameter Analysis. *ACS Appl. Mater. Interfaces* **2015**, *7* (14), 7801–7808.
- (93) Philippe, B.; Valvo, M.; Lindgren, F.; Rensmo, H.; Edström, K. Investigation of the Electrode/Electrolyte Interface of Fe<sub>2</sub>O<sub>3</sub> Composite Electrodes: Li vs Na Batteries. *Chem. Mater.* **2014**, *26*, 5028–5041.
- (94) Chen, K.; Song, S.; Xue, D. Faceted Cu<sub>2</sub>O Structures with Enhanced Li-Ion Battery Anode Performances. *CrystEngComm* **2015**, *17* (10), 2110–2117.
- (95) Neumann, J. P.; Zhong, T.; Chang, Y. A. The Cu-O (Copper-Oxygen) System. *Bull. Alloy Phase Diagrams* **1984**, *5* (2), 136–140.
- (96) Wang, F.; Robert, R.; Chernova, N. A.; Pereira, N.; Omenya, F.; Badway, F.; Hua, X.; Ruotolo, M.; Zhang, R.; Wu, L.; et al. Conversion Reaction Mechanisms in Lithium Ion Batteries: Study of the Binary Metal Fluoride Electrodes. *J. Am. Chem. Soc.* **2011**, *133*, 18828–18836.
- (97) Okoshi, M.; Yamada, Y.; Yamada, A.; Nakai, H. Theoretical Analysis on De-Solvation of Lithium, Sodium, and Magnesium Cations to Organic Electrolyte Solvents. *J. Electrochem. Soc.* **2013**, *160* (11), A2160–A2165.
- (98) Sagane, F.; Abe, T.; Ogumi, Z. Sodium-Ion Transfer at the Interface between Ceramic and Organic Electrolytes. *J. Power Sources* **2010**, *195* (21), 7466–7470.
- (99) Hartmann, P.; Heinemann, M.; Bender, C. L.; Graf, K.; Baumann, R.-P.; Adelhelm, P.; Heiliger, C.; Janek, J. Discharge and Charge Reaction Paths in Sodium-Oxygen Batteries: Does NaO<sub>2</sub> Form by Direct Electrochemical Growth or by Precipitation from Solution? *J. Phys. Chem. C* **2015**, *119*, 22778–22786.
- (100) Arcelus, O.; Li, C.; Rojo, T.; Carrasco, J. Electronic Structure of Sodium Superoxide Bulk, (100) Surface, and Clusters Using Hybrid Density Functional: Relevance for Na-O<sub>2</sub> Batteries. *J. Phys. Chem. Lett.* **2015**, *6* (11), 2027–2031.
- (101) Yang, S.; Siegel, D. J. Intrinsic Conductivity in Sodium–Air Battery Discharge Phases: Sodium Superoxide vs Sodium Peroxide. *Chem. Mater.* **2015**, *27* (11), 3852–3860.
- (102) Lim, Y.-F.; Chua, C. S.; Lee, C. J. J.; Chi, D. Sol-Gel Deposited Cu<sub>2</sub>O and CuO Thin Films for Photocatalytic Water Splitting. *Phys. Chem. Chem. Phys.* **2014**, *16* (47), 25928–25934.
- (103) Pouston, S.; Parlett, P. M.; Stone, P.; Bowker, M. Surface Oxidation and Reduction of CuO and Cu<sub>2</sub>O Studied Using XPS and XAES. *Surf. Interface Anal.* **1996**, *24* (June), 811–820.
- (104) Espinós, J. P.; Morales, J.; Barranco, A.; Caballero, A.; Holgado, J. P.; González-Elipe, A. R. Interface Effects for Cu, CuO, and Cu<sub>2</sub>O Deposited on SiO<sub>2</sub> and ZrO<sub>2</sub>. XPS Determination of the Valence State of Copper in Cu/SiO<sub>2</sub> and Cu/ZrO<sub>2</sub> Catalysts. *J. Phys. Chem. B* **2002**, *106*, 6921–6929.
- (105) Biesinger, M. C.; Lau, L. W. M.; Gerson, A. R.; Smart, R. S. C. Resolving Surface Chemical States in XPS Analysis of First Row Transition Metals, Oxides and Hydroxides: Sc, Ti, V, Cu and Zn. *Appl. Surf. Sci.* **2010**, *257* (3), 887–898.
- (106) Stevens, D. A.; Dahn, J. R. The Mechanisms of Lithium and Sodium Insertion in Carbon Materials. *J. Electrochem. Soc.* **2001**, *148* (8), A803–A811.
- (107) Morales, J.; Sánchez, L.; Martín, F.; Ramos-Barrado, J. R.; Sánchez, M. Use of Low-Temperature Nanostructured CuO Thin Films Deposited by Spray-Pyrolysis in Lithium Cells. *Thin Solid Films* **2005**, *474* (1–2), 133–140.
- (108) Moretti, G. Auger Parameter and Wagner Plot in the Characterization of Chemical States by X-Ray Photoelectron Spectroscopy: A Review. *J. Electron Spectrosc. Relat. Phenom.* **1998**, *95*, 95–144.
- (109) Morales, J.; Sánchez, L.; Martín, F.; Ramos-Barrado, J. R.; Sánchez, M. Nanostructured CuO Thin Film Electrodes Prepared by Spray Pyrolysis: A Simple Method for Enhancing the Electrochemical Performance of CuO in Lithium Cells. *Electrochim. Acta* **2004**, *49* (26), 4589–4597.
- (110) Chen, K.; Xue, D. Room-Temperature Chemical Transformation Route to CuO Nanowires toward High-Performance Electrode Materials. *J. Phys. Chem. C* **2013**, *117* (44), 22576–22583.
- (111) Su, Q.; Yao, L.; Zhang, J.; Du, G.; Xu, B. In Situ Transmission Electron Microscopy Observation of the Lithiation–Delithiation Conversion Behavior of CuO/Graphene Anode. *ACS Appl. Mater. Interfaces* **2015**, *7*, 23062–23068.
- (112) Wang, X.; Tang, D.-M.; Li, H.; Yi, W.; Zhai, T.; Bando, Y.; Golberg, D. Revealing the Conversion Mechanism of CuO Nanowires during Lithiation–delithiation by in Situ Transmission Electron Microscopy. *Chem. Commun.* **2012**, *48* (40), 4812.
- (113) Balaya, P.; Li, H.; Kienle, L.; Maier, J. Fully Reversible Homogeneous and Heterogeneous Li Storage in RuO<sub>2</sub> with High Capacity. *Adv. Funct. Mater.* **2003**, *13* (8), 621–625.
- (114) Zhukovskii, Y. F.; Kotomin, E. A.; Balaya, P.; Maier, J. Enhanced Interfacial Lithium Storage in Nanocomposites of Transition Metals with LiF and Li<sub>2</sub>O: Comparison of DFT Calculations and Experimental Studies. *Solid State Sci.* **2008**, *10* (4), 491–495.
- (115) Balaya, P.; Bhattacharyya, A. J.; Jamnik, J.; Zhukovskii, Y. F.; Kotomin, E. A.; Maier, J. Nano-Ionics in the Context of Lithium Batteries. *J. Power Sources* **2006**, *159* (1), 171–178.
- (116) Laruelle, S.; Gruegeon, S.; Poizot, P.; Dollé, M.; Dupont, L.; Tarascon, J.-M. On the Origin of the Extra Electrochemical Capacity Displayed by MO/Li Cells at Low Potential. *J. Electrochem. Soc.* **2002**, *149* (5), A627.
- (117) Gruegeon, S.; Laruelle, S.; Dupont, L.; Tarascon, J.-M. An Update on the Reactivity of Nanoparticles Co-Based Compounds towards Li. *Solid State Sci.* **2003**, *5* (6), 895–904.

- (118) Dedryvère, R.; Laruelle, S.; Grugeon, S.; Poizot, P.; Gonbeau, D.; Tarascon, J.-M. Contribution of X-Ray Photoelectron Spectroscopy to the Study of the Electrochemical Reactivity of CoO toward Lithium. *Chem. Mater.* **2004**, *16*, 1056–1061.
- (119) Gireaud, L.; Grugeon, S.; Pilard, S.; Guenot, P.; Tarascon, J.-M.; Laruelle, S. Mass Spectrometry Investigations on Electrolyte Degradation Products for the Development of Nanocomposite Electrodes in Lithium Ion Batteries. *Anal. Chem.* **2006**, *78* (11), 3688–3698.
- (120) Gachot, G.; Grugeon, S.; Armand, M.; Pilard, S.; Guenot, P.; Tarascon, J.-M.; Laruelle, S. Deciphering the Multi-Step Degradation Mechanisms of Carbonate-Based Electrolyte in Li Batteries. *J. Power Sources* **2008**, *178* (1), 409–421.
- (121) Dollé, M.; Poizot, P.; Dupont, L.; Tarascon, J.-M. Experimental Evidence for Electrolyte Involvement in the Reversible Reactivity of CoO toward Compounds at Low Potential. *Electrochem. Solid-State Lett.* **2002**, *5* (1), A18.
- (122) Ponrouch, A.; Taberna, P.-L.; Simon, P.; Palacín, M. R. On the Origin of the Extra Capacity at Low Potential in Materials for Li Batteries Reacting through Conversion Reaction. *Electrochim. Acta* **2012**, *61*, 13–18.
- (123) Ponrouch, A.; Cabana, J.; Dugas, R.; Slack, J. L.; Palacín, M. R. Electroanalytical Study of the Viability of Conversion Reactions as Energy Storage Mechanisms. *RSC Adv.* **2014**, *4* (68), 35988–35996.
- (124) Laruelle, S.; Pilard, S.; Guenot, P.; Grugeon, S.; Tarascon, J.-M. Identification of Li-Based Electrolyte Degradation Products Through DEI and ESI High-Resolution Mass Spectrometry. *J. Electrochem. Soc.* **2004**, *151* (8), A1202–A1209.
- (125) Dedryvère, R.; Gireaud, L.; Grugeon, S.; Laruelle, S.; Tarascon, J.-M.; Gonbeau, D. Characterization of Lithium Alkyl Carbonates by X-Ray Photoelectron Spectroscopy: Experimental and Theoretical Study. *J. Phys. Chem. B* **2005**, *109* (33), 15868–15875.
- (126) Dedryvère, R.; Laruelle, S.; Grugeon, S.; Gireaud, L.; Tarascon, J.-M.; Gonbeau, D. XPS Identification of the Organic and Inorganic Components of the Electrode/Electrolyte Interface Formed on a Metallic Cathode. *J. Electrochem. Soc.* **2005**, *152* (4), A689–A696.
- (127) Dupont, L.; Laruelle, S.; Grugeon, S.; Dickinson, C.; Zhou, W.; Tarascon, J.-M. Mesoporous Cr<sub>2</sub>O<sub>3</sub> as Negative Electrode in Lithium Batteries: TEM Study of the Texture Effect on the Polymeric Layer Formation. *J. Power Sources* **2008**, *175* (1), 502–509.
- (128) Zeng, Y.; Li, L.; Li, H.; Huang, X.; Chen, L. TG-MS Analysis on Thermal Decomposable Components in the SEI Film on Cr<sub>2</sub>O<sub>3</sub> Powder Anode in Li-Ion Batteries. *Ionics* **2009**, *15* (1), 91–96.